WYLE LABORATORIES
SCIENTIFIC SERVICES AND SYSTEMS GROUP
EASTERN OPERATIONS
FACILITIES LOCATED IN
HUNTSVILLE, ALA. AND HAMPTON, VA.

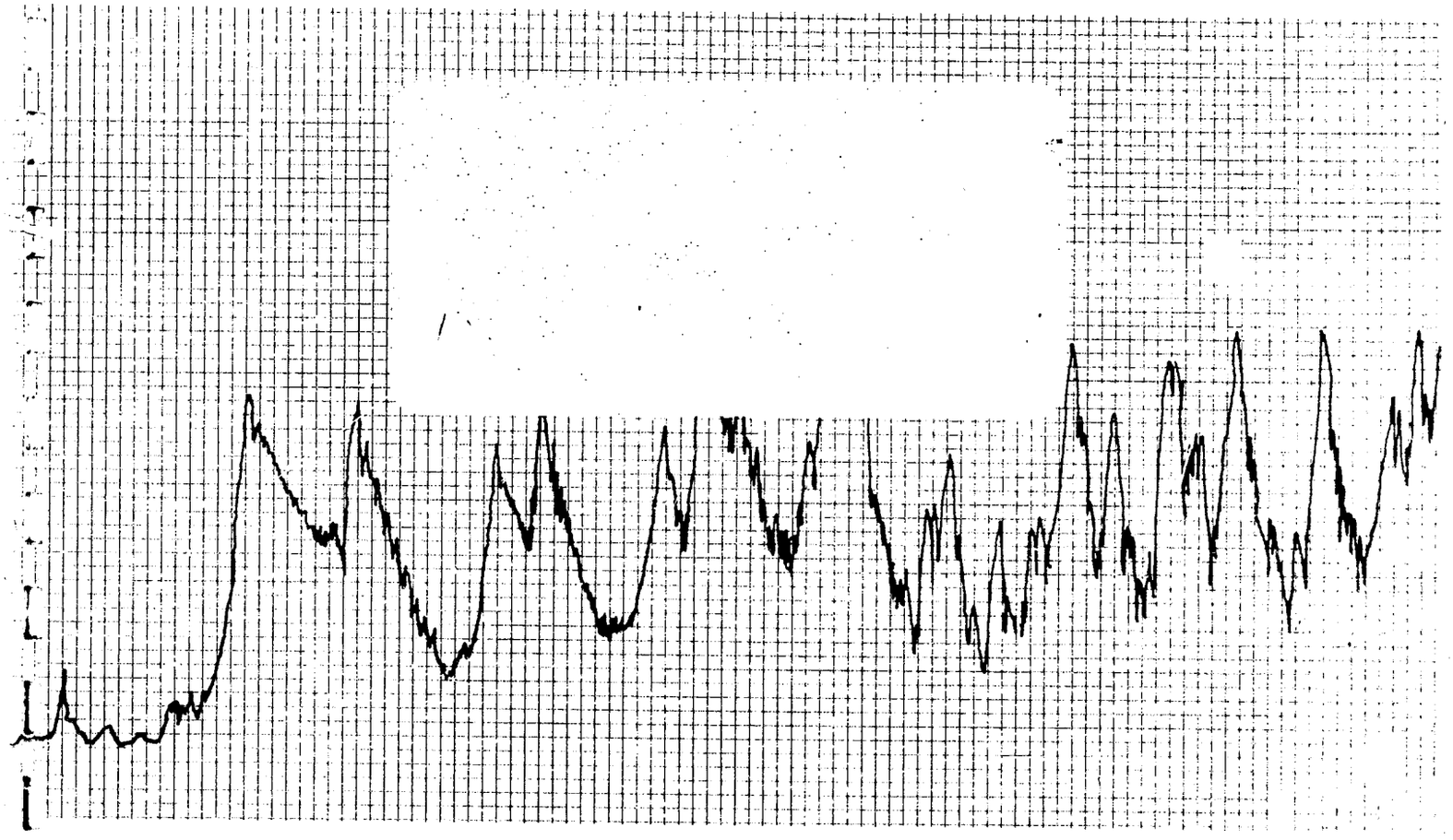

research REPORT

WYLE LABORATORIES — RESEARCH STAFF
REPORT WR 73-3

PREDICTION OF FLUCTUATING PRESSURE ENVIRONMENTS ASSOCIATED WITH PLUME-INDUCED SEPARATED FLOW FIELDS

By

Kenneth J. Plotkin

May 1973

Work Performed Under Contract No. NAS8-26919

WYLE LABORATORIES

COPY NO. 9

ABSTRACT

The separated flow environment induced by underexpanded rocket plumes during boost phase of rocket vehicles has been investigated. A simple semi-empirical model for predicting the extent of separation was developed. This model offers considerable computational economy as compared to other schemes reported in the literature, and has been shown to be in good agreement with limited flight data. The unsteady pressure field in plume-induced separated regions was investigated. It was found that fluctuations differed from those for a rigid flare only at low frequencies. The major difference between plume-induced separation and flare-induced separation was shown to be an increase in shock oscillation distance for the plume case. The prediction schemes were applied to PRR shuttle launch configuration. It was found that fluctuating pressures from plume-induced separation are not as severe as for other fluctuating environments at the critical flight condition of maximum dynamic pressure.

TABLE OF CONTENTS

LIST OF FIGURES

LIST OF FIGURES (Continued)

LIST OF FIGURES (Concluded)

NOMENCLATURE

a_∞	Sound speed
d	Local thickness of separated region
D	Plume drag
f	Frequency
f_0	Frequence corresponding to macroscale of spectrum
f_{sep}	Separation region response frequency
f_{pl}	Plume response frequency
H	Boundary layer shape factor
ℓ_s	Separation length
L	Vehicle length
M	Mach number
p	Pressure
p_c	Engine chamber pressure
r_p	Plume nose radius
r_v	Vehicle radius
R_e	Reynolds number
T	Engine thrust
u	Speed
u_c	Convection velocity
u_∞	Free stream speed
x	Streamwise coordinate

γ	Ratio of specific heats
δ	Boundary layer thickness
δ_0	Boundary layer thickness immediately upstream
δ_i^*	Boundary layer displacement thickness in transformed coordinates
θ_i	Boundary layer momentum thickness in transformed coordinates
θ_{pl}	Plume angle at nozzle lip
θ_{reat}	Reattachment turning angle
θ_{sep}	Separation angle
Φ	Spectral density
$( )_s$	Condition at separation point
$( )_{BL}$	Condition in attached turbulent boundary layer
$( )_{sep}$	Condition in separated region
$( )_{sw}$	Condition at shock wave location
$\langle \rangle$	Average

1.0 INTRODUCTION

During atmospheric flight, the external surfaces of the space shuttle vehicles will be subjected to high intensity acoustic and fluctuating pressure environments. Wyle Laboratories is engaged in a research program under NASA-MSFC Contract NAS8-26919 to develop reliable methods of predicting critical acoustic and fluctuating pressure environment trends during space shuttle flight. In the course of this program, fluctuations associated with various attached and separated flow environments have been defined and quantitative prediction formulae developed (References 1-7). Among the most severe fluctuating environments are those associated with compression induced separated flow and shock oscillation. These are associated with protuberances and flares in the vehicle geometry, and, as described below, exhaust plumes.

During the boost phase of atmospheric flight, engine exhaust material forms an effective afterbody. When the exhaust is highly underexpanded (nozzle exit pressure much greater than free-stream pressure) the resultant plume can be significantly larger than the vehicle itself. Under these conditions, compression induced separation may exist over a significant area of the vehicle due to plume interference. When the Reynolds number is high enough so that the flow field may be treated as inviscid flow plus boundary layer (with strong interactions occurring only locally at separation points), plume effects may be treated by considering the plume to be an afterbody whose surface corresponds to the dividing streamline between exhaust material and the ambient. Calculation of the flow field is more difficult than for a rigid body because the plume shape is implicitly dependent on the pressure field. Because the equivalent plume "body" is a dividing streamline and may respond to pressure fluctuations, the fluctuating flow environment cannot be assumed a priori to correspond exactly to that of a rigid afterbody.

In this report, the fluctuating pressures associated with plume induced separation are examined. The basic properties of supersonic flow separation and of highly underexpanded rocket plumes are first discussed, and an approximate model for separation length and steady properties is presented. Although more elaborate models may provide more accurate predictions of separation lengths, the simple model employed clearly exhibits the overall scaling properties of plume-induced separation. The flow properties deduced from this model are then applied to the known properties of fluctuating pressures associated with separation by rigid flared bodies.

Anticipated departures from these properties due to the non-rigid nature of the plume are identified. These include fluctuations of the plume itself due to combustion instabilities. Finally, predictions of boost phase plume-induced fluctuating pressures are made for a preliminary shuttle configuration and mission.

2.0 PLUME-INDUCED SEPARATED FLOW FIELDS

The basic flow configuration of interest is illustrated in Figure 1. There are three distinct regions: exhaust flow, outer separated flow, and recirculation region. The turning angles of the outer flow at the separation point and reattachment point are governed by viscous interaction: the turning angle must be consistent with the increase in boundary layer displacement thickness. The locations of the slip lines are determined by pressure matching. The reattachment point is located such that the pressure rise across the inner plume shock equals the pressure rise across the reattachment shock. Boger, Rosenbaum and Reeves (Reference 8) and Fong (Reference 9) have developed computer programs to calculate the separation induced flow field for an initially laminar boundary layer. The individual components of the flow field shown in Figure 1 are discussed in detail in the following subsections.

2.1 Viscous Separating and Reattaching Flows

The problem of separation of supersonic flows is an important one for high speed vehicles, and has been the subject of a number of theoretical and experimental investigations. Figures 2 and 3 show two supersonic configurations leading to separated flow: an impinging shock wave in Figure 2, and a compression corner in Figure 3. An important feature of both flows is that information of compression is propagated upstream through the boundary layer. Without a boundary layer, the separation region would degenerate into a point — the shock impingement point in Figure 2 or the corner in Figure 3. It is clear, therefore, that compression-induced separation is a viscous interaction phenomenon.

Various theoretical treatments have shown that boundary layers may be supercritical or subcritical. In a subcritical boundary layer, disturbances are communicated upstream; in a supercritical layer they are not. There is a direct analogy to subsonic and supersonic flow. In the case of a supercritical boundary layer, communication of a pressure rise can be achieved only through a "jump" to subcritical, just as with a shock wave. After reattachment, the layer goes through a neck region where a transition from subcritical to supercritical takes place. Crocco and Lees (Reference 10) showed that the correct solution for reattachment is one which passes smoothly through this critical point.

Theoretical approaches have generally been to use the integral form of the boundary layer equations. Early studies were for simple methods, such as Karman-Pohlhausen, with more sophisticated methods being gradually adopted. Theoretical development was also first for laminar boundary layers (Reference 11), being modified later to include turbulent layers. The most recent theoretical model of turbulent separation is due to Hunter and Reeves (Reference 12) and Todisco and Reeves (Reference 13). In this model, the laminar sublayer and skin friction are neglected, so that the flow is wake-like. This appears to be a reasonable approximation, as skin friction does vanish at separation. Boundary layer behavior at distances upstream of separation does not affect this model as virtually all attached supersonic turbulent boundary layers are supercritical (Reference 14).

The model developed by Todisco and Reeves and extended by Hunter and Reeves applies to the separated flow configuration of Figure 3. A set of supercritical-subcritical jump conditions (analogous to normal shock relations) were found for the separation point. After separation, development of the free shear layer is calculated by numerical integration of the moment integral form of the boundary layer equations. Shear layer profiles are expressed as a one parameter function of shape factor $H = \theta_i / \delta_i^*$, where θ_i and δ_i^* are momentum and displacement thickness, respectively, in transformed coordinates. After reattachment, the pressure is assumed to be the inviscid wedge pressure corresponding to the wedge angle. The wedge angle is adjusted until the solution passes smoothly through the critical point.

Figure 4 shows a typical result obtained by Todisco and Reeves. Flow conditions are noted on the figure. A separation shock with pressure ratio of about 2 (this does not increase markedly, even at hypersonic Mach numbers) is followed by a rise to plateau pressure. At the corner, pressure rises more sharply, approaching ramp pressure downstream of the critical point.

The variation of plateau pressure with Mach number is shown in Figure 5, along with some experimental data. According to the Todisco and Reeves theory, plateau pressure is independent of ramp angle. This has been questioned — at least for the hypersonic case — by Elfstrom (Reference 15). Figure 6(a) shows plateau pressures measured by Elfstrom added to Figure 5. Figure 6(b) shows this data normalized with respect to inviscid ramp pressure, with apparently excellent collapse. However, Reeves (Reference 16) has pointed out that all of Elfstrom's

measurements are for separation lengths no greater than 4 boundary layer thicknesses; at such small lengths, pressure at the corner has not reached plateau conditions. Reeves presents plots (Figure 7) which show reasonable agreement when p/p_∞ is collapsed according to $\Delta x/\delta_0$. Most available data appears to be for separation lengths $\ell_s/\delta_0 < 8$, at which point plateau conditions are still not reached. Reeves pointed out that experiments capable of providing data for ℓ_s/δ_0 at least 15 should be performed, and would settle this question. For the present, it appears that Reeves' interpretation of the data is supported by the Todisco-Reeves theory, and will therefore be adopted in this report.

An interesting feature of turbulent separation is that Reynolds number dependence is very weak, becoming negligible for Reynolds number greater than two or three times the value at transition (Reference 17). This would appear at first to be peculiar for a viscous interaction phenomenon. However, it should be noted that at high enough Reynolds numbers the inertial subrange will dominate the turbulence spectrum, so that viscosity itself has a less important role. This is consistent with, for example, the empirical correlation for turbulent boundary layer thickness (Reference 18)

$$\delta = x \left[0.37 R_e^{-0.2} \left\{ 1 + \left(\frac{R_e}{6.9 \times 10^7} \right)^2 \right\}^{0.1} \right] \qquad (1)$$

which becomes $\delta = 0.01x$ at large R_e. This is a considerable simplification over laminar separation, in which Reynolds number remains an important parameter. Separation of a turbulent supersonic boundary layer should depend only on local boundary layer properties and Mach number. For zero pressure gradient, only Mach number remains as an important parameter. For the purpose of this report, therefore, separation plateau pressure will be taken as that given by the Todisco-Reeves theory, shown in Figure 5, and separation angle based on tangent wedge for this pressure.

2.2 Plume Flow Field

Figure 8 illustrates the inviscid flow field of a supersonic highly underexpanded rocket plume. Region I is free-stream flow. Flow in Region IV is exhaust flow, and is the same flow as would exist in a vacuum. Flow in Regions I and IV must both turn in order to match pressure and direction at the contact surface; since both flows are supersonic, they will experience shock waves. Flow within Region II has been turned outward by the outer plume shock, with the flow in Regions I and II being the same as for a body with shape corresponding to the interface. Flow in Region IV is turned by the barrel shock so that flow in Region III is more in the axial direction. Since pressure in Region IV diminishes rapidly downstream as the vacuum flow expands radially, the barrel shock must increase in strength with downstream distance. At the nozzle lip, where engine exhaust simply expands isentropically until it matches pressure at the interface, the barrel shock has zero strength; far downstream it becomes stronger, approaching the hypersonic limit. At some point downstream the barrel shock terminates at a normal shock, generally referred to as the Mach disc. A series of "cells", similar to the Mach diamonds of a slightly overexpanded jet, may exist beyond this; however, for the present problem only the forward portion of this first cell is of interest.

In the case of a plume in a quiescent ambient, Region II does not exist and Region I has zero velocity and constant pressure. Calculation of the plume flow field is then a straightforward matter using the method of characteristics, and has been done by a number of investigators, including References 19 and 20. When the ambient is flowing, the pressure becomes a function of the interface shape. If conditions are such that the outer shock is attached to the nozzle lip and the flow is everywhere supersonic, a method of characteristics calculation should present no difficulties, although the calculation would be more complex because exhaust material and ambient have different properties.

At very high altitudes, the initial exhaust expansion at the nozzle lip is great enough so that an attached outer shock cannot exist (Reference 21); in this case the bow shock is detached and Region II corresponds to the flow about a blunt body. Supersonic blunt body flow calculations are difficult enough with a known body shape. The combination of a state of the art blunt body computer program with a method of characteristics program presents formidable difficulties and has not yet been done.

Because a computation of high speed plume flow fields using the most advanced techniques presents great difficulties, calculations to date have used various approximate methods. Boynton (Reference 22) has employed a Lagrangian (stream tube) finite difference method. It is not ideal for supersonic flows, as Boynton points out, because it does not implicitly contain the wave nature of such flows and shock waves present special problems. Its main advantage is providing some answer where no other exists. Another approach is to use Newtonian flow to locate the dividing streamline (References 23 and 24). The primary disadvantage of this method is that the inner shock is very weak near the nose of the plume, so that Newtonian flow is not a very good approximation for the nose portion of Region III.

Although detailed calculations of plume flow fields have not yer been entirely successful, certain scaling properties have been well established. Jarvinen and Hill (Reference 25) have developed a semi-empirical "universal plume profile" which incorporates these scaling laws. Figure 9 shows the Jarvinen-Hill model. Dimensions in the axial direction scale as $(T/q_\infty)^{\frac{1}{2}}$, where T = rocket thrust and q_∞ is freestream dynamic pressure. Dimensions in the lateral direction scale as $((TD)^{\frac{1}{2}}/q_\infty)^{\frac{1}{2}}$, where D = plume drag. Plume drag is defined as the vacuum thrust which would result if the exhaust were fully expanded, minus the actual vacuum thrust. The physical interpretation of this quantity may be seen if the interface is imagined to be a nozzle wall; D is simply the total aerodynamic force exerted on the plume material. The universal plume profile shown in Figure 9 is based on experimental data, method of characteristics computation and Newtonian flow computations, with the nose region based on a blast wave analogy.

The Jarvinen-Hill plume profile provides a good working model except for the very nose, where detail necessarily neglected by such a model is important. The parabolic nose resulting from the blast wave analogy implies a 90° turning angle of exhaust at the nozzle lip; this is generally not correct. The initial angle of the plume is, however, simple to compute. Reis, et al. (Reference 20) noted that, for plumes into a quiescent ambient, only one family of characteristics entered the computation very near the nozzle lip. This means that the inner flow for a very short distance from the lip can be determined by a Prandtl-Meyer expansion. If the outer flow pressure is obtained by Newtonian flow or tangent cone, the

initial angle of the contact surface is easily obtained. The universal plume profile can then be modified to include the actual angle for each set of flight conditions.

2.3 Plume-Induced Separation

Boger, Rosenbaum and Reeves (Reference 8) (hereinafter called BRR) and Fong (Reference 9) have recently published schemes for computing plume-induced separation. The BRR scheme is described in Section 2.3.1: Fong's scheme is roughly similar but more elaborate, including the shear layer at the plume interface as well as the separation line. A simplified scheme is presented in Section 2.3.2.

2.3.1 Separation Scheme of Boger, Rosenbaum and Reeves — The BRR scheme follows the basic elements outlined in Section 2.0: separation and reattachment are governed by viscous interaction, with the plume boundary determined by an inviscid calculation. The numerical scheme follows four steps:

1) A separation point is assumed. Separation angle, plateau pressure and Mach number corresponding to plateau pressure are determined. The example used in Reference 8 was for an initially laminar attached boundary layer; plateau pressure was computed using a relation from Reference 26; angle and Mach number were obtained from this by tangent-cone.

2) Using the plateau pressure, the plume boundary is computed by the method of characteristics. Because plateau pressure is constant, this was done by a scheme developed for computing plumes in a quiescent ambient. Neglecting the viscous layer at the plume boundary in determining the boundary is justified by a series of wind tunnel experiments reported in Reference 8 . The plume boundary, separation angle, and assumed separation point give a preliminary reattachment point on the plume boundary.

3) The turning angle at reattachment is determined from the viscous interaction theory of Todisco and Reeves (Reference 13). For a given plateau Mach number and shape factor $H = \theta_i / \delta_i^*$, the turning angle is uniquely determined. Figure 10 shows the conditions used by BRR. At the separation point $H = H_s$, so that $H/H_s = 1$; as the shear layer develops, H/H_s decreases, approaching zero for a fully developed free shear layer.

4) The pressure after reattachment is known from the turning angle determined in Step 3. The point on the plume boundary which gives the same pressure after turning to the same final angle is located. If this point does not agree with the point from Steps 1 and 2, a new separation point consistent with this is chosen. The four steps are iterated until the solution converges.

The BRR scheme as described here requires recomputation of the plume boundary at each iteration only if plateau conditions are dependent on separation point. For a smooth body with zero pressure gradient at the separation point, this means a dependence on Reynolds number. The laminar example presented in Reference 8 has a Reynolds number dependence. For a turbulent attached boundary layer at very large Reynolds number, as described in Section 2.1, there is no Reynolds number dependence. Iteration of the separation point is still required, however, because the reattachment conditions depend on the length of the shear layer.

2.3.2 Approximate Model for Plume-Induced Separation — The BRR scheme appears to be a reasonable method for computing plume-induced separation. However, there are certain approximations in calculating the separated flow. The most significant is assuming constant pressure in the plateau region. As seen in Figure 4, this is clearly not the case: pressure varies somewhat after separation, and considerably after the corner. This latter is crucial, as it is the assumption of constant pressure that enables a characteristics solution of the plume flow. A proper calculation, taking the pressure gradient into account would be of the same difficulty as the hypersonic plume with detached bow shock discussed earlier. Other approximations, such as assuming a constant separation angle, are not as significant as this.

Since the boundary conditions for the method of characteristics plume calculation are not correct, it is worth seeing if further approximations are possible so as to eliminate entirely the need for it. As this is the most complex part of the BRR scheme, it would greatly simplify computation. Toward this end, the following assumptions are made:

1) As with BRR, pressure within the separation region is assumed constant.

2) The plume boundary adjacent to the separation region is adequately described by a Prandtl-Meyer expansion to match plateau pressure. The contact surface is thus conical in this region. This is the same model as used in Reference 21 to predict detachment of the outer plume shock.

3) Outside of the separated region, the Jarvinen-Hill universal plume profile is adequate to describe the contact surface. In the nose region, the surface is a sphere with radius r_p.

With these assumptions in hand, the plume-induced separation flow model is shown in Figure 11. The separation angle θ_{sep} and plateau pressure and Mach number are given by the Todisco–Reeves theory, θ_{pl} is found by expanding exhaust flow to match plateau pressure, and $r_p = 0.2\ (D/q_\infty)^{\frac{1}{2}}$ is from the Jarvinen-Hill plume model. The reattachment turning angle, the separation point and center of spherical interface are such that the reattachment angle $(\theta_{sep} + \theta_{reat})$ is tangent to the sphere at the reattachment point. The separation length is then given by

$$\ell_s = \left[r_p \cos (\theta_{sep} + \theta_{reat}) - r_v \right] \left(\cot \theta_{sep} - \cot \theta_{pl} \right) \qquad (2)$$

For typical vehicles of interest here, the boundary layer is fully developed turbulent. Separation pressure is therefore given by Figure 5, with Mach number and angle determined from the wedge flow charts of Reference 27. Separation values at $M < 2$ were extrapolated. The values of M_{sep} and θ_{sep} used are shown in Figure 12.

Because the vehicles of interest, and consequently separation lengths, are very large, it is expected that the separated shear layer at reattachment will be close to fully developed. Therefore, reattachment conditions are taken as given by the curve for $H/H_s = 0.11$ on Figure 10. This curve is chosen because it is the most developed case presented in Reference 8. Figure 13 shows this curve extrapolated down to Mach numbers of interest here.

A computer program, described in Appendix A, was written to compute separation conditions versus time for any given flight trajectory. The program includes fluctuating conditions, developed in Section 3.0, as well as steady separation conditions discussed thus far.

As an example of this simplified calculation, separation conditions were calculated for the Saturn V S-1, using a nominal Apollo launch trajectory (Reference 28). Trajectory parameters are shown in Figure 14. Figure 15 shows the predicted separation point versus time after lift off. Data (Reference 29) obtained from a microphone at station 757 on an Apollo flight indicated large fluctuating pressure of the type associated with shock wave oscillation from approximately 118 seconds to approximately 130 seconds. This range is indicated on Figure 15; the separation point passes station 757 somewhere during this time period. Since the shock wave precedes the separation point by a small amount, the separation point most likely passes this station somewhat after the middle of this time range. Agreement between this data point and the prediction is good. The prediction method presented in this section for plume-induced separation is therefore quite adequate to use as a framework for estimating fluctuating pressure environments.

3.0 FLUCTUATIONS IN PLUME-INDUCED SEPARATED ENVIRONMENTS

3.1 Summary of Fluctuating Pressure Environment in a Compression Corner

Figure 16, from Reference 30, shows the static and fluctuating pressure environments ahead of a compression corner. The fluctuating pressure may be divided into three parts: incoming boundary layer, shock wave oscillation, and homogeneous separated flow. The spectra associated with each of these are shown in Figure 17. Reference 4 reviews available data and provides empirical prediction schemes for these environments. The amplitudes and spectra shown in Figures 16 and 17 are representative of two dimensional and axisymmetric compression induced separation; the scaling parameters used in these figures were found in Reference 4. to give best collapse of experimental data. Application of prediction schemes to specific vehicle configurations is straightforward, and shows excellent agreement with wind tunnel measurements (Reference 7).

Although empirical predictions of fluctuating properties can be made with some confidence, the fundamental mechanism involved are not fully understood for all parts of the flow. The following properties, relative to assessing the effect of the free plume boundary, are established:

3.1.1 Turbulent Boundary Layer — This is the best understood part of the flow. Since supersonic turbulent boundary layers are generally supercritical, boundary layer properties upstream of the separation point will not be affected by the plume boundary.

3.1.2 Shock Wave Oscillation — An analytical model has been established linking the motion of the shock wave to fluctuations in the incoming turbulent boundary layer (Reference 6). The shock wave is convected by velocity fluctuations in the boundary layer. Since boundary layer fluctuations may be treated as a stochastic process, the shock wave executes a random walk about its mean location. Mean flow properties seek to return the shock to its mean location, so that displacement is limited. At large times, the shock motion is a stationary random process with mean square displacement dependent on both boundary layer fluctuations and the mean flow restoring mechanism. The macroscale of the displacement is governed by the mean flow restoring mechanism. Conditions within the separation region may therefore influence the shock motion. For example, slowly varying fluctuating pressure in the

exhaust flow would cause the separation length, hence shock location, to fluctuate. (For exhaust oscillations slow compared to response time of the separated flow, shock motion may be calculated as quasi-steady.) For a steady exhaust flow, it is expected that the nature of the shock motion (driven by the boundary layer) will not change, but that the total excursion may.

3.1.3 Separated Flow Region — No quantitative model has yet been developed for this region. Even mean flow conditions are not yet fully established (Reference 15). However, the fluctuating flow is qualitatively understood and arguments may be put forth as to the mechanisms of the fluctuations.

The mean flow in a compression corner has been partly described in Section 2.1, and is shown in Figure 3. A key feature of the flow for interpreting fluctuations is the region beneath the separation streamline. In the discussion of Section 2.1, this was treated essentially as a "dead water" region. As with most "dead water" regions, it is actually a recirculation zone, with trapped eddies. For two-dimensional and axisymmetric flows, there is a single large eddy in the separation region. This eddy is a key factor in the fluctuating pressure field, expecially at low frequencies. With a single trapped eddy, two-dimensional and axisymmetric flows should have similar fluctuating pressures; this is borne out by Figures 16 and 17. Separated flow induced by three-dimensional protuberances, on the other hand, exhibits different (and larger) fluctuating pressure levels (Figure 18). This is clearly a consequence of the multiple trapped eddy structure, identified by Robertson's oil flow experiments (Reference 2). For the present problem, only two-dimensional and axisymmetric flows are of interest. However, it should be noted that the turbulent boundary layer and shock oscillation fluctuations are essentially the same for protuberances as for two-dimensional flow. This is in agreement with the conclusions of Sections 3.1.1 and 3.1.2.

Interpretation of fluctuations in the separation region requires knowledge of narrow band convection velocities. Figure 19 shows convection velocities presented by Coe and Rechtien (Reference 30). Convection velocities presented by Chyu and Hanley (Reference 31) and Rechtien (Reference 32) are essentially the same.

Reference 32 does indicate negative convection velocities at very low frequencies (approximately $f\delta/u_\infty < 0.03$), but there is considerable scatter in that range. Because of the scatter, and because low frequency random data is inherently less accurate than higher frequencies, it is not clear whether or not negative convection velocities really exist. The phase angle of the cross-correlation function is also near zero in this range, which makes accurate calculation of convection speed difficult.

The convection velocities shown in Figure 19 vary from a minimum of $u_c/u_\infty \approx 0.2$ at $f\delta/u_\infty \approx 0.06$ to a plateau $u_c/u_\infty \approx 0.8$ at $f\delta/u_\infty \approx 0.8$. Shown for comparison with the plateau are convection velocities obtained by Bull (Reference 33) for attached turbulent boundary layers. Agreement with the plateau above $f\delta/u_\infty = 0.8$ is good. Noting that eddies of size δ convected at $u_c = 0.8\, u_\infty$ correspond to $f\delta/u_\infty = 0.8$, it may be concluded that fluctuations at high frequencies, $f\delta/u_\infty \geq 0.8$, are associated with the free shear layer. Rechtein (Reference 32) provides qualitative arguments that pressure fluctuations in this frequency range are transmitted to the wall by the "eddy Mach wave" phenomenon (Reference 34). For the present purposes, however, it is sufficient to only identify this frequency range with the free shear layer. It may then be concluded that this part of the fluctuations will not be affected by having a non-rigid plume boundary downstream.

For $f\delta/u_\infty < 0.8$, attached boundary layer convection velocities slowly rise, approaching u_∞ as $f\delta/u_\infty \rightarrow 0$ (Reference 33), while convection speed in the separation corner decreases. This difference is because low frequency boundary layer noise is identified with free stream air entrained at the edge of the layer, while the free shear layer entrains nearly still air from the separation bubble under it.

Convection velocities for $f\delta/u_\infty < 0.8$ can be interpreted in terms of a simple entrainment model. The free shear layer is initially composed of eddies of size δ, convected at $u_c = 0.8\, u_\infty$. Essentially still air beneath it is entrained, with the vorticity of the original layer distributed over the entire layer. If the thickness of the layer is now d, eddy sizes are also of size d. The convection speed of the larger eddies is

$$u_c = 0.8\, u_\infty \frac{\delta}{d} \qquad (3)$$

This represents conservation of momentum of the original layer. The frequency associated with a series of eddies of size d moving at speed u_c is

$$f = \frac{u_c}{d}$$

so that

$$\frac{f\delta}{u_\infty} = \frac{u_c}{d}\,\frac{\delta}{u_\infty} = 0.8\left(\frac{\delta}{d}\right)^2 \qquad (4)$$

Figure 20 shows a model convection speed, based on boundary layer convection for $f\delta/u_\infty \geq 0.8$ and Equations (3) and (4) for $f\delta/u_\infty \leq 0.8$. Also shown are convection speeds from Figure 19. Agreement of this simple entrainment model is quite good for $f\delta/u_\infty$ larger than about 0.1, which corresponds to $d/\delta \approx 3$. In the experiments of Reference 30, step height was not more than a few boundary layer thicknesses. Since the entrained layer cannot be thicker than approximately the step height (and must be somewhat less because there must be a reverse flow near the wall), it is not expected that this entrainment model would apply at lower frequencies than this.

The agreement between convection speeds for the entrainment model and the data indicates that fluctuations in this frequency range are also generated by the shear layer. The plume boundary should therefore have no major effect on fluctuations above $f\delta/u_\infty \approx 0.1$.

The convection velocity has a minimum of about $0.2\,u_\infty$ at $f\delta/u_\infty = 0.06$, then rises sharply below that. It is in the region of this rise that Rechtein (Reference 32) obtained widely scattered positive and negative convection velocities. Since a solenoidal pulsation would result in infinite positive and negative computed convection speeds, it may be concluded that the region $f\delta/u_\infty < 0.06$ is dominated by large scale fluctuations of the whole separation bubble. This conclusion may be supported by considering the acoustic response frequency of the separation bubble. If the separation length is 10δ (experimental measurements cited here are generally less) and $M = 2$, then the fundamental response of a cavity of equal size

corresponds to $f\delta/u_\infty = 0.05$. This is approximately where large scale fluctuations begin to dominate over the convected eddies. In this range, it is expected that there will be coupling between the plume boundary and fluctuating separation pressure.

3.2 Coupling Between Plume Boundary and Separation Fluctuations

The discussion of Section 3.1 leads to the conclusion that above a certain frequency separated flow fluctuations are dependent primarily on the incoming turbulence. Below this frequency, the geometry of the mean flow (i.e., the actual dimensions of the separation region) has a direct effect on fluctuations. It is in this frequency range that flow over a plume may differ from flow over a rigid flare.

Because the feedback mechanism through the plume interface involves motion of the plume, it is necessary to assess the response of the plume to pressure fluctuations. There will be some frequency (based on characteristic flow time of the plume) below which the plume will exhibit direct response, following pressure fluctuations quasi-statically. Coupling of motion in this regime will be relatively straightforward. At higher frequencies, response of the plume will lag somewhat, with direct feedback being less as fluctuation frequency increases.

In Section 3.2.1 below, the various characteristic frequencies are summarized and the frequency range of separated flow fluctuation/plume boundary coupling identified. The quantitative effect on fluctuating pressure environments are then estimated in Section 3.2.2.

3.2.1 Frequency Range of Fluctuation/Plume Coupling — The "fundamental" frequency of a separated region of length ℓ_s is

$$f_{sep} = \frac{a_\infty}{2\ell_s} \tag{5}$$

where it is assumed that sound speed within the separated region is a_∞. This is the first acoustic mode of a cavity of size ℓ_s. At frequencies less than f_{sep}, pressure fluctuations are in phase. This corresponds to the infinite convection speeds discussed in Section 3.1.3.

Casting f_{sep} in the form $f\delta_0/u_\infty$,

$$f_{sep}\delta_0/u_\infty = \frac{a_\infty}{2\ell_s}\frac{\delta_0}{u_\infty}$$

$$= \frac{1}{2M_\infty}\frac{\delta_0}{\ell_s} \qquad (6)$$

The value of $f_{sep}\delta_0/u_\infty$ given by Equation (6) corresponds to the lower frequency limit of convected fluctuations, as discussed in Section 3.1.3. It was concluded in that section that at frequencies greater than f_{sep} the presence of a non-rigid plume boundary does not influence separated flow fluctuations.

For the plume interface to follow pressure fluctuations quasi-statically, the plume flow time must be greater than the fluctuation flow time. The plume flow time is given by the length of plume interface within the separated region, divided by flow speed. For the present purposes, the length may be taken as $\ell_s \tan\theta_{sep}$ and the speed as u_e. For typical separation angles $\tan\theta_{sep} \approx 1/4$, so that the response frequency of the plume is

$$f_{pl} = \frac{4u_e}{\ell_s}$$

Casting in the form $f\delta_0/u_\infty$,

$$f_{pl}\delta_0/u_\infty = 4\frac{u_e}{u_\infty}\frac{\delta_0}{\ell_s} \qquad (7)$$

Comparing Equations (6) and (7),

$$f_{pl} = 8 \frac{u_e}{u_\infty} \frac{1}{M_\infty} f_{sep} \tag{8}$$

so that f_{pl} is generally an order of magnitude larger than f_{sep}. This means that at frequencies where pressure fluctuations are coupled to the plume motion, the plume boundary response is quasi-steady. This is an important finding, and much simplifies calculation of the response.

The frequencies given by Equations (6) and (7) must be compared to characteristic frequencies of the fluctuating flow. The most important frequencies are those corresponding to the integral scales of the fluctuation spectra. The bulk of the overall fluctuating pressure level is identified with a frequency band about this value.

The integral time scale of a fluctuating environment is defined in Reference 6; the corresponding frequency is the reciprical of the time. For the spectra shown in Figure 17, the characteristic frequencies for the boundary layer, separated region, and shock wave oscillation are

$$f_{0_{BL}} \delta_0 / u_\infty = 0.53 \tag{9a}$$

$$f_{0_{sep}} \delta_0 / u_\infty = 0.145 \tag{9b}$$

$$f_{0_{sw}} \delta_0 / u_\infty = 0.04 \tag{9c}$$

Figure 21 shows Equations (6), (7) and (9) as a function of ℓ_s/δ_0. Also indicated is ℓ_s/L, separation length divided by total vehicle length. This was obtained by assuming δ_0 is given by the large Reynolds number limit of Equation (1), and noting that distance from the front of the vehicle is $L - \ell_s$, so that

$$\delta_0 = 10^{-2} (L - \ell_s) \tag{10}$$

Comparison of the various curves in Figure 21 leads to the following conclusions:

- Except for small separation lengths ($\ell_s/\delta_0 < 1$ at $M_\infty = 2$, for example), overall fluctuating pressure level in the separation region is not affected.

- For $\ell_s/\delta_0 \lesssim 10$, shock wave motion may be strongly coupled to plume motion. It should be noted that shock oscillation is not a homogeneous environment, so that important low frequency effects may occur at larger separation lengths as well. However, although these effects may be important, it is not expected that overall levels will change significantly.

- Boundary layer fluctuations upstream of separation, and high frequency fluctuations in the separation region, will not be affected.

3.2.2 Amplitude of Coupling — For all important frequencies, plume response to separation fluctuations will be quasi-static. The plume size changes in response to separation pressure fluctuations. The separation point and shock wave then move in accordance with the instantaneous plume size.

The mean square pressure fluctuation in the separation region is

$$\langle p^2 \rangle = \int_0^\infty \Phi_{sep}(f)\, df \tag{11}$$

Feedback to the separated region is only for $f \delta_0 / u_\infty \leq 1/M_\infty \; \delta_0 / \ell_s$; the pressure fluctuation in this frequency range is

$$\Delta \langle p^2 \rangle = \int_0^{a_\infty / \ell_s} \Phi_{sep}(f) \, df \tag{12}$$

Equation (12) has been numerically integrated, using the analytic representation of Φ_{sep} presented in Reference 4. The quantity $\Delta \langle p^2 \rangle^{\frac{1}{2}} / \langle p^2 \rangle^{\frac{1}{2}}$ is plotted as a function of $M \ell_{sep} / \delta_0$ in Figure 22. Figure 23 shows $\Delta \langle p^2 \rangle^{\frac{1}{2}} / q_\infty$ as a function of ℓ_{sep} / δ_0 for several Mach numbers, based on Figure 22 and the Mach number dependence of $\langle p^2 \rangle^{\frac{1}{2}} / q_\infty$ as presented in Reference 4. The quantity $\Delta \langle p^2 \rangle^{\frac{1}{2}} / q_\infty$ may be considered to be the "feedback fluctuating pressure coefficient", since it represents that part of the fluctuating pressure which can couple directly to the plume.

The response of the plume to the feedback fluctuating pressure is straightforward to compute. Referring to Figure 11, θ_{sep}, θ_{reat} and r_p are functions of the external flow only, so that the only change in geometry is through changes in θ_{pl}. If θ_{pl} changes by an amount $\Delta\theta_{pl}$, the separation length changes by

$$\Delta \ell_s = \frac{\ell_s}{\cot \theta_{sep} - \cot \theta_{pl}} \tan \Delta\theta_{pl} \left[\frac{1 + \cot^2 \theta_{pl}}{1 + \tan \Delta\theta_{pl} \cot \theta_{pl}} \right] \tag{13}$$

For small changes in $\Delta\theta_{pl}$, such that $\tan \Delta\theta_{pl} \ll 1$, Equation (13) may be represented as

$$\Delta \ell_s = \frac{d\ell_s}{d\theta_{pl}} \Delta\theta_{pl} \tag{14}$$

where

$$\frac{d\ell_s}{d\theta_{pl}} = \frac{\ell_s}{\cot\theta_{sep} - \cot\theta_{pl}} \left[1 + \cot^2\theta_{pl}\right] \tag{15}$$

Root mean square change in separation length due to change in plateau pressure is given by

$$\left(\Delta\ell_s{}^2\right)^{\frac{1}{2}} = \frac{d\ell_s}{d\theta_{pl}} \frac{d\theta_{pl}}{d\left(p/q_\infty\right)} \frac{\left(\Delta\langle p^2\rangle\right)^{\frac{1}{2}}}{q_\infty} \tag{16}$$

where $d\theta_{pl} / d\,(p/q_\infty)$ must be obtained for the plume flow field. Since θ_{pl} is obtained by a Prandtl-Meyer expansion of the exhaust flow to match plateau pressure, it is straightforward to obtain

$$\frac{d\,\theta_{pl}}{d\,p/q_\infty} = \frac{q_\infty}{p_c} \frac{\sqrt{M^2-1}}{\gamma\, M^2} \left(1 + \frac{\gamma-1}{2}\, M^2\right)^{\gamma/\gamma-1} \tag{17}$$

where M is the Mach number of the exhaust flow after expanding to θ_{pl}. Equation (17) is obtained by differentiating Equations (2.31) and (4.21b) of Reference 36.

All parameters needed for Equations (15) and (17) are available from the calculation of separation length. Figure 24 shows $d\ell_s / d\,(p/q_\infty)$ versus Time After Lift-Off for the Saturn V, nominal Apollo trajectory. Using the feedback fluctuating pressure coefficient shown in Figure 23, the change in separation length has been calculated. Figure 25 shows the increase in root mean square separation length due to the flexible plume boundary; shown for comparison are boundary layer thickness and root mean square shock oscillation displacement for an equivalent rigid flare. The net rms shock motion will be no greater than $\langle x_{sw}^2\rangle^{\frac{1}{2}} + \langle \Delta\ell^2\rangle^{\frac{1}{2}}$ (this represents perfect coherence between x_{sw} and $\Delta\ell$). Figure 26

shows $\langle \Delta \ell_s^2 \rangle^{\frac{1}{2}} / \langle x_{sw}^2 \rangle^{\frac{1}{2}}$ for the Saturn V. The increase in rms shock wave displacement is less than 23 percent. Fluctuating pressure at the shock wave is proportional to displacement (Reference 6); the rms fluctuating pressure level at the shock location is therefore increased from $0.068\, q_\infty$ (Reference 6) to $0.0836\, q_\infty$. On the decibel scale, this is an increase of 2 dB.

Other than the slightly increased fluctuating level at the shock location, the change in separation length is not enough to significantly alter the fluctuating pressure patterns. It may therefore be concluded that, for the example presented, there is little difference between fluctuations associated with flare-induced separation and plume-induced separation. The only significant difference is a slight increase in shock oscillation distance and fluctuating level.

The analysis so far has assumed that the exhaust flow itself is steady. The question of unsteady exhaust is treated in the next section. What may be concluded here is that the fluctuating pressure due to plume-induced separation does not have an important coupling effect itself with the plume boundary. Homogeneous fluctuating pressure environments may therefore be superposed on fluctuating pressures associated with unsteady plume effects discussed in the next section. Pressure fluctuations due to the oscillating shock wave, which is an inhomogeneous environment, does not simply superpose; however, once the displacement is known the shock oscillation pressure field can be determined from the theory of Reference 6.

3.3 Plume Driven Fluctuations

The discussion thus far has assumed that the engine exhaust flow is steady, with turbulent fluctuations present only in the external separated flow. For real rocket engines this is not the case. At the high pressures and Reynolds numbers involved, flow within the combustion chamber is turbulent. Further, the combustion process, with vaporizing fuel droplets burning, is not uniform. Although the nature of fluctuations within a rocket engine can be of several types (Reference 35), for the present purposes only the effect of a solenoidal pulsing of combustion chamber pressure will be evaluated.

3.3.1 Low Frequency Fluctuations: Quasi-Static Response — If all other parameters are held fixed, thrust and exit pressure of a rocket engine are proportional to chamber pressure. For chamber pressure fluctuations of frequency less than f_{pl} as shown in Figure 21, the fluctuating plume shape may be computed quasi-statically, with $T/\langle T \rangle = p_e/\langle p_e \rangle = p_c/\langle p_c \rangle$. Referring to Figure 11, the model plume shape will experience changes in θ_{pl} and r_p due to thrust fluctuations. The angles θ_{sep} and θ_{reat} are unchanged. The plateau pressure is assumed to be unchanged; this assumption is correct for $f < f_{sep}$, when separation region response is also quasi-static.

For small changes in θ_{pl} and r_p, the change in separation length is:

$$\Delta \ell_s = \frac{\partial \ell_s}{\partial \theta_{pl}} \Delta\theta_{pl} + \frac{\partial \ell_s}{\partial r_p} \Delta r_p \tag{18}$$

where $\partial \ell_s/\partial\theta_{pl}$ is the same as $d\ell_s/d\theta_{pl}$ given in Equation (15), and

$$\frac{\partial \ell_s}{\partial r_p} = \cos\left(\theta_{sep} + \theta_{reat}\right)\left(\cot\theta_{sep} - \cot\theta_{pl}\right) \tag{19}$$

For small fluctuations in chamber pressure and thrust, $\Delta\theta_{pl}$ and Δr_p are

$$\Delta\theta_{pl} = \frac{\partial\theta_{pl}}{\partial T/\langle T\rangle} \frac{\Delta T}{\langle T\rangle} \tag{20a}$$

$$\Delta r_p = \frac{\partial r_p}{\partial T/\langle T\rangle} \frac{\Delta T}{\langle T\rangle} \tag{20b}$$

Note that any appearance of $\Delta T/\langle T \rangle$ in Equation (20) can be replaced by $\Delta p_c/\langle p_c \rangle$.

The plume radius used in the present model, described in Section 2.3.2, is

$$r_p = 0.2 \left(\frac{D}{q_\infty} \right)^{\frac{1}{2}} \tag{21}$$

Plume drag D is proportional to thrust T; thus, for small fluctuations in T,

$$\frac{\partial r_p}{\partial T/\langle T \rangle} = \frac{1}{2} r_p \tag{22}$$

The change in plume angle θ_{pl} is governed by matching the Prandtl-Meyer expansion of the fluctuating exhaust flow to the constant plateau pressure. Derivation of $d\theta_{pl} / d p_c/\langle p_c \rangle$ is similar to derivation of Equation (17), except that Equation (2.31) of Reference 38 is differential with respect to p_c rather than p . The result is

$$\frac{d \theta_{pl}}{dp_c/\langle p_c \rangle} = \frac{\sqrt{M^2 - 1}}{(\gamma-1) M^2} \tag{23}$$

where M is the Mach number of the exhaust flow after expanding to θ_{pl} .

Combining Equations (18) through (23),

$$\Delta \ell_s = \frac{d \ell_s}{dp_c/\langle p_c \rangle} \frac{\Delta p_c}{\langle p_c \rangle} \tag{24}$$

where

$$\frac{d\ell_s}{dp_c/\langle p_c \rangle} = \frac{\partial \ell_s}{\partial \theta_{pl}} \frac{M^2-1}{(\gamma-1)M^2} + \frac{\partial \ell_s}{\partial r_p} \frac{1}{2} r_p \qquad (25)$$

where $\partial \ell_s / \partial \theta_{pl}$ and $\partial \ell_s / \partial r_p$ are given by Equations (15) and (19).

Figure 28 shows Equation (25) for the Saturn V. Little data is available on fluctuating thrust of the F-1 engine; however, if thrust fluctuates by 1%, separation length would vary by approximately 0.5 meter. As with the fluctuations discussed in Section 3.2, variations of separation length of this order do not significantly affect the homogeneous separated flow fluctuations. Fluctuations due to the increased motion of the shock wave can be accounted for by applying the theory of Reference 6.

3.3.2 High Frequency Fluctuations: Acoustic Response — At plume fluctuation frequencies $f > f_{sep}$, response time of the separated flow is slower than fluctuation of the plume. The separated region therefore does not respond quasi-statically to the plume motion. In the high frequency limit, $f \gg f_{sep}$, the separation region may be considered to be steady (except, of course, for the pre-existing fluctuations which have been shown to be essentially independent of the plume), with plume fluctuations transmitted as acoustic disturbances. The fluctuating pressure in the separated region is then comprised of:

- Fluctuation as described in Section 3.1, modified according to Section 3.2.
- Low frequency fluctuations where the separated flow responds quasi-statically to plume fluctuations, as discussed in Section 3.3.1.
- High frequency acoustic fluctuations superposed on the environment obtained from the first two above.

This last environment represents the jet noise of the rocket exhaust, and should be treated as a separate acoustic environment, rather than a part of plume-induced separation environments. The connection between this and separation is that the separation region provides a medium for upstream noise propagation at supersonic speeds. The model discussed so far does indicate that the acoustic environment may be divided into two regimes, which are worth pointing out at this time:

- For $f_{sep} < f < f_{pl}$, the plume interface within the separated region may be considered to move solenoidally. The acoustic disturbance, within the context of the Lighthill theory (Reference 37), is then a distribution of synchronous sources along the plume interface.

- For $f > f_{pl}$, the inhomogeneity of the plume must be accounted for. The sound source is then a distribution of quadrupoles. In this regime, the acoustic field must be treated as a full near-field jet noise problem.

4.0 APPLICATION TO SHUTTLE PRR CONFIGURATION

4.1 Shuttle Flow Field

Figure 28 shows the PRR shuttle configuration. It is comprised of four separate units linked together: an orbiter, an external tank, and two solid rocket boosters (SRB). The flow field for the mated launch vehicle will consist of the individual flow fields of each major body, with modifications due to interference between bodies. Because of the complexity of this vehicle, extensive theoretical and experimental studies will be required to accurately define the actual flow over the mated bodies.

Despite the complexity of the interference regions of the shuttle flow field, there are some major areas where the flow will be simple enough so as to permit application of the simple axisymmetric plume model developed in this report. For zero angle of attack, the flow over the outboard sections of the SRB should be adequately described by locally axisymmetric flow about the centerline of each SRB. Provided the radii of the individual plumes are small enough so that they do not mutually interfere to a significant degree, the axisymmetric plume separation model developed in Section 2.0 may then be applied to the outboard section of the SRB with the same degree of confidence as the application to Saturn V separation presented earlier.

To a lesser degree, the axisymmetric separation model may also be applied to the top surface of the orbiter. There is no direct interference in this region. However, the orbiter alone is not axisymmetric, the flow up to the flat top surface is over a relatively complex three-dimensional body, and the aft region is cluttered by the presence of the OMS/RCS pods and a vertical control surface. Therefore, although this calculation is performed below, the results should be considered to be an indication of trends rather than a quantitative prediction of separation point on the orbiter.

4.1.1 Plume-Induced Separation on SRB — To compute separation on the outboard side of the SRB, each SRB is treated as a single axisymmetric vehicle at zero angle of attack. The pertinent vehicle parameters for the SRB of the PRR configuration are summarized in Table I, based on data presented in References 38 and 39.

TABLE I

SRB PARAMETERS	
Vehicle Radius	81 in. = 2.06 m
Thrust	4, 162, 204 lb = 18.5×10^6 N
γ_{ex}	1.145
Nozzle Area Ratio	10
Exhaust Mach Number	3.18
Chamber Pressure	680 psia = 4.68×10^6 N/m^2

Plume separation and fluctuation parameters were calculated for the due East trajectory used in Reference 7, shown in Figure 29. The results are shown in Figures 30 through 33.

Figure 30 shows plume-induced separation length. Separation begins at about 95 seconds (altitude = 18 km, $M_\infty = 1.8$, $q_\infty = 18{,}500$ N/m^2), and encompasses the entire SRB at SRB cut-off of 145 seconds (altitude = 45 km, $M_\infty = 4.6$). Note that separation does not occur until well after conditions of maximum dynamic pressure, 82 seconds, altitude = 13 km, $M_\infty = 1.332$, $q_\infty = 22{,}460$ N/m^2. Comparing dynamic pressure, it may be concluded that, unless fluctuating pressure coefficients in the plume separation region are greater than 1.33 times those of flare-induced separation, plume-induced separation will not introduce more severe fluctuating pressure environments than those at the critical condition of maximum dynamic pressure.

Figure 31 shows $d\ell_s/(dp/q_\infty)$. Using the feedback pressure coefficient shown in Figure 23, the change in separation length was obtained. Figure 32 shows $\langle \Delta \ell_s^2 \rangle^{\frac{1}{2}}$, the increase in separation length due to the flexible plume boundary, along with boundary layer thickness at the separation point and root mean square displacement for an equivalent rigid flare. At the onset of separation, $\langle \Delta \ell_s^2 \rangle^{\frac{1}{2}}$ is slightly less than $\langle x_{SW}^2 \rangle^{\frac{1}{2}}$, so that for perfect coherence shock oscillation distance is almost double that for a flare. Doubling oscillation distance would no more than double fluctuating pressure, or an increase of 6 dB. Adding 6 dB to the prediction presented in Reference 7 (and using the correct dynamic pressure for 95 seconds),

shock oscillation levels at the onset of separation will be approximately 161 dB. This is 3 dB higher than shock oscillation level of 158 dB predicted at maximum q_∞ in Reference 7, and 4 dB less than protuberance-induced homogeneous fluctuating pressure level of 165 dB at maximum q_∞.

Fluctuating pressure levels in the homogeneous separated region will be the same as for a rigid flare, hence will not be as great as those experienced at the critical condition of maximum q_∞.

Figure 33 shows the change of separation length with fluctuation in engine chamber pressure. This prediction may be applied when data on SRB chamber pressure fluctuations are available.

4.1.2 Plume-Induced Separation on Orbiter — For the purpose of estimating separation trends, the present prediction scheme has been applied to the shuttle orbiter. The calculation was performed for an axisymmetric vehicle of radius comparable to orbiter dimensions. The vehicle and engine parameters used are listed in Table II.

TABLE II

ORBITER PARAMETERS	
Vehicle Radius	122 in. = 3.11 m
Thrust	1.4×10^6 lb = 6.2×10^6 N
γ_{ex}	1.23
Nozzle Area Ratio	35
Exhaust Mach Number	4.05
Chamber Pressure	3000 psia = 2.065×10^7 N/m^2

Figure 34 shows predicted separation length. Note that at 145 seconds, corresponding to SRB cut-off, the predicted separation point has not yet extended beyond the OMS/RCS pods and vertical control surface. This cluttered region is expected to experience protuberance-induced fluctuations and interference effects; therefore, plume induced separation will not make the

flow environment more severe. At later times, dynamic pressure is low enough that separated flow fluctuating pressures are not important. Therefore, it may be concluded that plume-induced separation due to the orbiter engines is not an important factor evaluating fluctuating flow environments.

5.0 CONCLUSIONS

The separated flow environment induced by underexpanded rocket plumes during boost phase of rocket vehicles has been investigated. A simple model for predicting the extent of separation was developed. The model employs a semi-empirical geometric representation of the plume interface. It was concluded that this simple representation, rather than a numerical method of characteristics computation as employed by other investigators, is sufficiently refined so as to be consistent with other approximations generally employed in the calculation of plume-induced separation. This simple model has the advantage of much greater economy of computation. Good agreement was found between present prediction of separation length and limited data from a Saturn V flight.

The unsteady pressure field in plume-induced separated regions was investigated. Emphasis was placed on determining differences between fluctuations associated with plume-induced separation and those associated with an equivalent rigid flare. The frequency domain of possible fluctuating pressure/plume boundary coupling was investigated. It was found that coupling is limited to low frequencies, below the characteristic frequencies associated with the homogeneous separated flow fluctuations. It was further found that the main effect of the plume is to allow greater shock wave excursion distances than for an equivalent rigid flare. Differences in pressure fluctuations are limited to those associated with shock wave oscillation, for which the plume environment is more severe. The quantitative difference was found to be a function of vehicle and engine characteristics and flight conditions. The trend is for differences between the two cases to become less as separation length increases.

The prediction scheme developed here has been applied to the PRR space shuttle configuration. The following results were found:

- Separation due to the SRB engine begins at approximately 18 km, and extends over most of the vehicle by SRB cut-off (45 km).

- Shock oscillation fluctuations associated with SRB plume-induced separation at the onset of separation are slightly less than 6 dB greater than those for an equivalent flare. At 18 km, the fluctuating pressure level is 161 dB; this

compares to maximum dynamic pressure (13 km) conditions of 158 dB for flare-induced shock oscillation and 165 dB for protuberance-induced separated flow.

- Shock oscillation levels exceed those for a rigid flare by lesser amounts as altitude increases above 18 km.

- Homogeneous separated flow pressure fluctuations induced by the SRB plume are comparable to those for a rigid flare.

- Separation due to the orbiter engines occurs at altitudes sufficiently high that it may be discounted as an important fluctuating pressure environment.

REFERENCES

1. Lowson, M.V., "Prediction of Boundary Layer Pressure Fluctuations," Wyle Laboratories Research Staff Report WR 67-15, October 1967.

2. Robertson, J.E., "Characteristics of the Static- and Fluctuating-Pressure Environments Induced by Three-Dimensional Protuberances at Transonic Mach Numbers," Wyle Laboratories Research Staff Report WR 69-3, June 1969.

3. Robertson, J.E., "Fluctuating Pressures Induced by Three-Dimensional Protuberances," Wyle Laboratories Research Staff Report WR 70-10, April 1970.

4. Robertson, J.E., "Prediction of In-Flight Flucutating Pressure Environments Including Protuberance Induced Flow," Wyle Laboratories Research Statf Report WR 71-10, March 1971.

5. Tu, Bo-Jang, "Prediction of Wall Pressure Fluctuations Beneath a Turbulent Boundary Layer Flow at Supersonic and Hypersonic Speeds," Wyle Laboratories Research Staff Report TM 71-3, September 1971.

6. Robertson, J.E., "Preliminary Estimates of Space Shuttle Fluctuating Pressure Environments," Wyle Laboratories Research Staff Report WR 72-10, August 1972.

7. Plotkin, Kenneth J., "Shock Wave Oscillation Driven by Turbulent Boundary Layer Fluctuations," Wyle Laboratories Research Staff Report WR 72-12, September 1972.

8. Boger, R.C., Rosenbaum, H., and Reeves, B.L., "Flowfield Interactions Induced by Underexpanded Exhaust Plumes," AIAA Journal 10, No. 3, pp. 300-306, March 1972.

9. Fong, Michael C., "An Analysis of Plume-Induced Boundary Layer Separation," J. Spacecraft and Rockets 8, No. 11, pp. 1107-1113, November 1971.

10. Crocco, L., and Lees, L., "A Mixing Theory for the Interaction Between Dissipative Flows and Nearly Isentropic Streams," J. Aero. Sci., 19, pp. 649-676, 1952.

11. Lees, Lester, and Reeves, B.L., "Supersonic Separated and Reattaching Laminar Flows: I. General Theory and Application to Adiabatic Boundary Layer/Shock-Wave Interactions," AIAA Journal 2, No. 11, pp. 1907-1920, November 1964.

12. Hunter, L.G., Jr., And Reeves, B.L., "Results of a Strong Interaction, Wake-Like Model of Supersonic Separated and Reattaching Turbulent Flows," AIAA Journal 9, No. 4, pp. 703-712, April 1971.

13. Todisco, A., and Reeves, B.L., "Turbulent Boundary Layer Separation and Reattachment at Supersonic and Hypersonic Speeds," Proceedings of Symposium on Viscous Interaction Phenomena in Supersonic and Hypersonic Flow, 1969, University of Dayton Press, pp. 139-179.

14. Crocco, L., and Probstein, R.F., "The Peak Pressure Rise Across an Oblique Shock Emerging from a Turbulent Boundary Layer over a Plane Surface," Princeton University, Aeronautical Engineering Dept., Report 254, March 1954.

15. Elfstrom, G.M., "Turbulent Hypersonic Flow at a Wedge-Compression Corner," J. Fluid Mech. 53, Part 1, pp. 113-127, 1972.

16. Reeves, B.L., "Plateau Pressure in Hypersonic Turbulent Boundary-Layer Interactions," AIAA Journal 10, No. 11, pp. 1546-1548, November 1972.

17. Zukoski, E.E., "Turbulent Boundary-Layer Separation in Front of a Forward-Facing Step," AIAA Journal 5, No. 10, pp. 1746-1753, October 1967.

18. Bies, D.A., "A Review of Flight and Wind Tunnel Measurements of Boundary Layer Pressure Fluctuations and Induced Structural Response," NASA CR-626, October 1966.

19. Vick, A.R., Andrews, E.H., Jr., Dennard, J.S. and Craidon, C.B., "Comparisons of Experimental Free-Jet Boundaries with Theoretical Results Obtained with the Method of Characteristics," NASA TN D-2327, June 1964.

20. Reis, R.J., Aucoin, P.J., and Stechman, R.C., "Prediction of Rocket Exhaust Flowfields," J. Spacecraft and Rockets 7, No. 2, pp. 155-159, February 1970.

21. Plotkin, Kenneth J., and Draper, James Stark, "Detachment of the Outer Shock from Underexpanded Rocket Plumes," AIAA Journal 10, No. 12, pp. 1707-1709, December 1972.

22. Boynton, F.P., "Highly Underexpanded Jet Structure: Exact and Approximate Calculations," AIAA Journal, Vol. 5, No. 9, September 1967, pp. 1703-1704.

23. Albini, F.A., "Approximate Computation of Underexpanded Jet Structure," AIAA Journal, Vol. 3, No. 8, August 1965, pp. 1535-1537.

24. Hubbard, E.W., "Approximate Calculation of Highly Underexpanded Jets," AIAA Journal, Vol. 4, No. 10, October 1966, pp. 1877-1879.

25. Jarvinen, P.O. and Hill, J.A.F., "Universal Model for Underexpanded Rocket Plumes in Hypersonic Flow," Proceedings of the 12th JANNAF Liquid Meeting, 1970, Las Vegas, Nevada.

26. Lewis, J.E., Kubota, T., and Lees, L., "Experimental Investigation of Supersonic Laminar, Two-Dimensional Boundary Layer Separation in a Compression Corner with and without Cooling," AIAA Journal 6, No. 1, pp. 7-14, January 1968.

27. Ames Research Staff, "Equations, Tables and Charts for Compressible Flow," Report 1135, 1953, NASA.

28. "Saturn V Performance and Trajectories," Marshall Space Flight Center, R-AERO-DAP-13-65, February 1965.

29. Jones, Jess H., "Acoustic Environment Characteristics of the Space Shuttle," NASA TM X-52876, pp. 285-297, July 1970.

30. Coe, C.F., and Rechtien, R.D., "Scaling and Spatial Correlation of Surface Pressure Fluctuations in Separated Flow at Supersonic Mach Numbers," Paper presented at the AIAA Structural Dynamics and Aeroelasticity Specialist Conference, New Orleans, Louisiana, April 16-17, 1969.

31. Chyu, W.J., and Hanly, R.D., "Power and Cross-Spectra and Space Time Correlation of Surface Fluctuating Pressures at Mach Numbers Between 1.6 and 2.5," AIAA Preprint No. 68-77, January 1968.

32. Rechtien, Richard D., "A Study of the Fluctuating Pressure Field in Regions of Induced Flow Separation at Supersonic Speeds," University of Missouri - Rolla UMR Research Report, May 1970.

33. Bull, M.K., "Wall Pressure Fluctuations Associated with Subsonic Turbulent Boundary Layer Flow," J. Fluid Mech. 28, Part 4, pp. 719-754, 1967.

34. Ffowcs Williams, J.E., and Maidanik, G., "The Mach Wave Field Radiated by Supersonic Turbulent Shear Flows," J. Fluid Mech. 21, Part 4, pp. 641-657, 1965.

35. Harrje, D.T., and Reardon, F.H., editors, "Liquid Propellant Rocket Combustion Instability," NASA SP-194, 1972.

36. Liepmann, H.W., and Roshko, A., Elements of Gasdynamics, Wiley, New York, 1957.

37. Lighthill, M.J., "On Sound Generated Aerodynamically — I. General Theory," Proc. Roy. Soc. Series A, 211, pp. 564-587, 1952.

38. Miller, J.Q., "Solid Rocket Motor," Space Shuttle External Tank and Solid Rocket Booster Quarterly Review, Marshall Space Flight Center, December 1972.

39. Miller, J.Q., "Shuttle Solid Rocket Motor," Space Shuttle External Tank and Solid Rocket Booster Quarterly Review, Marshall Space Flight Center, March 1973.

FIGURES

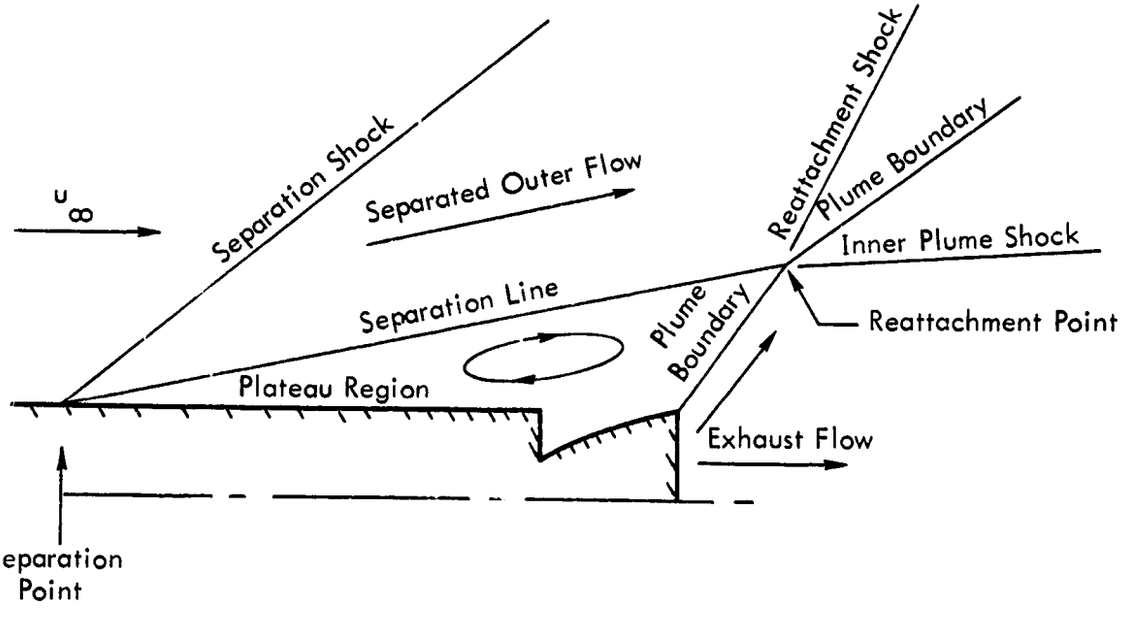

Figure 1. Plume Induced Separated Flow

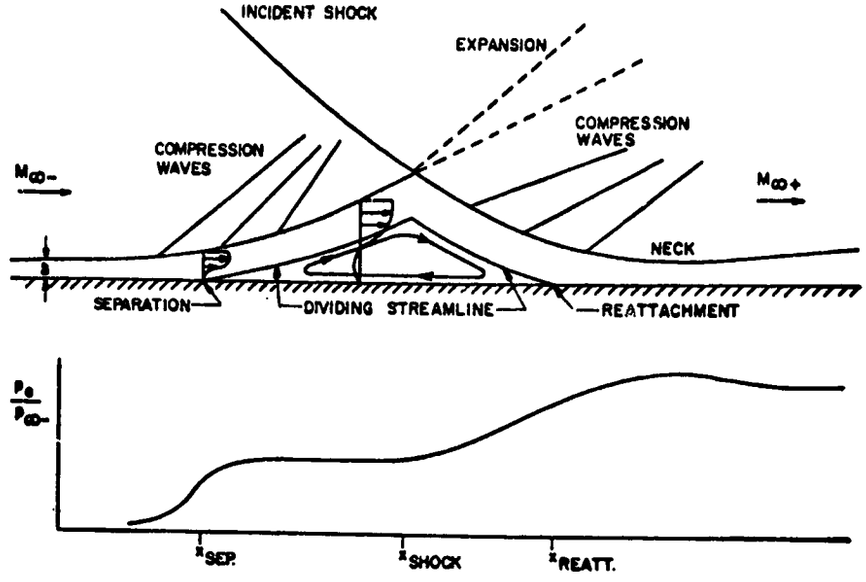

Figure 2. Schematic Representation of Shock-Wave/Laminar-Boundary-Layer Interaction, from Reference 11

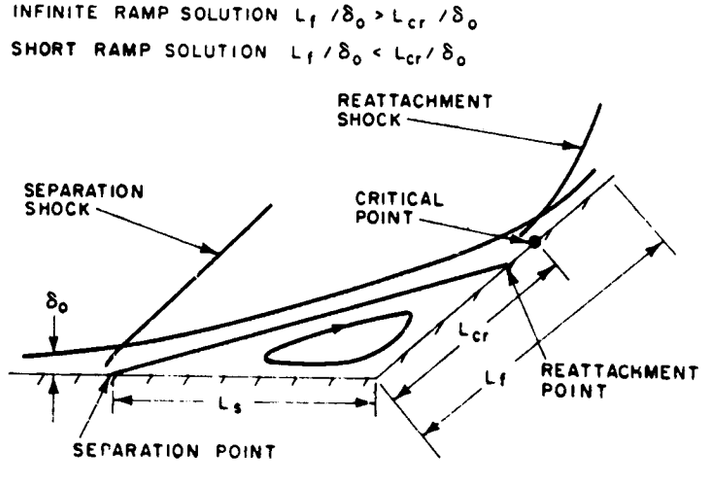

Figure 3. Schematic Representation of Turbulent Separated and Reattaching Flow, from Reference 12

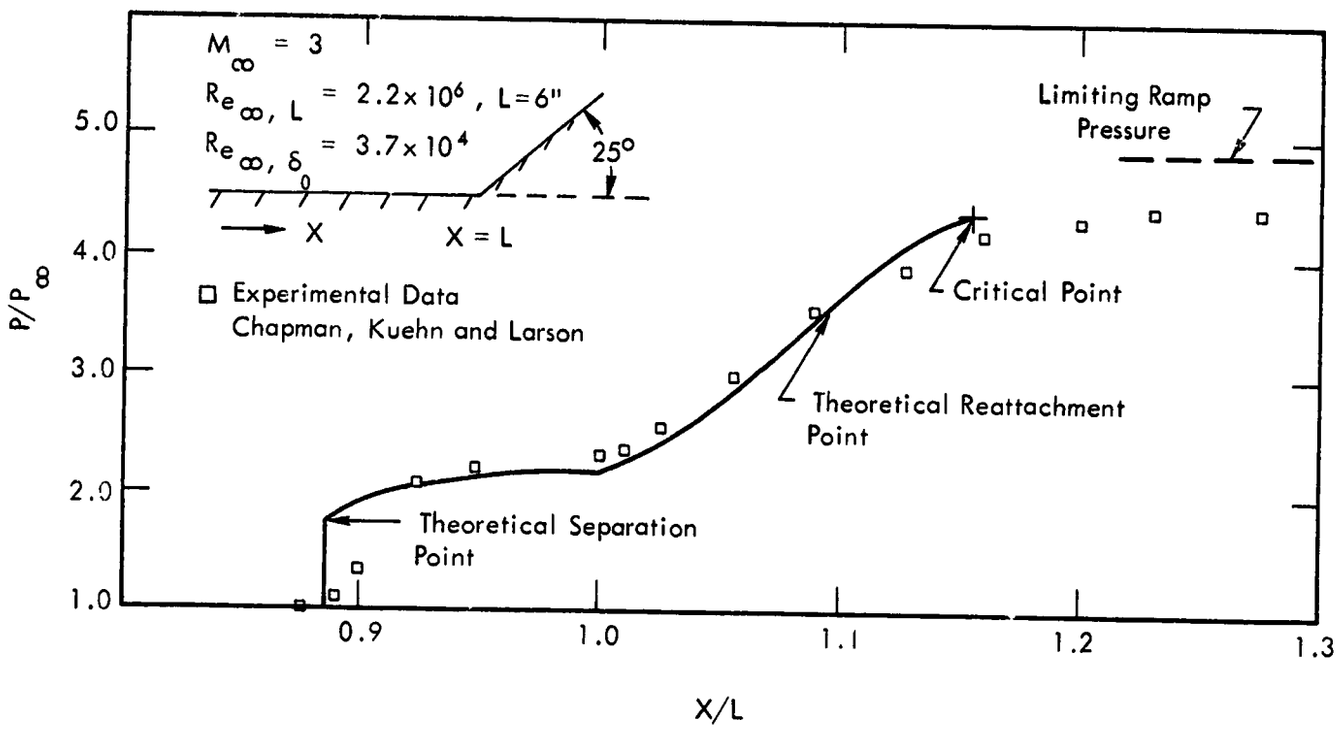

Figure 4. Pressure Distribution for 25° Compression Ramp, from Reference 13

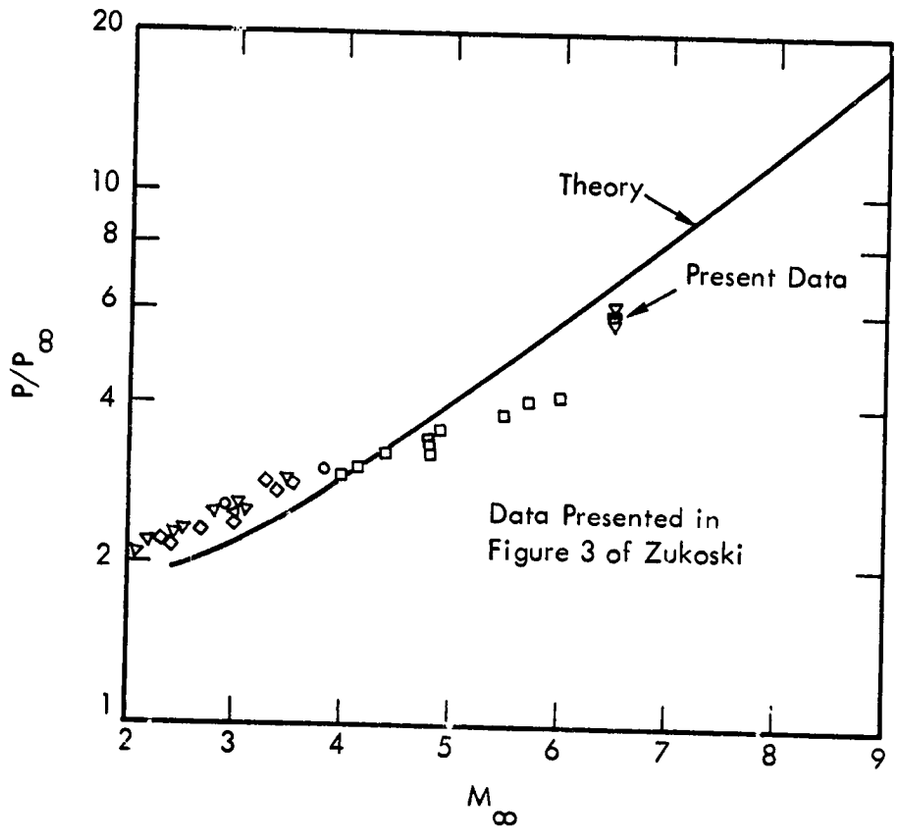

Figure 5. Variation of Plateau Pressure with Mach Number, from Reference 13

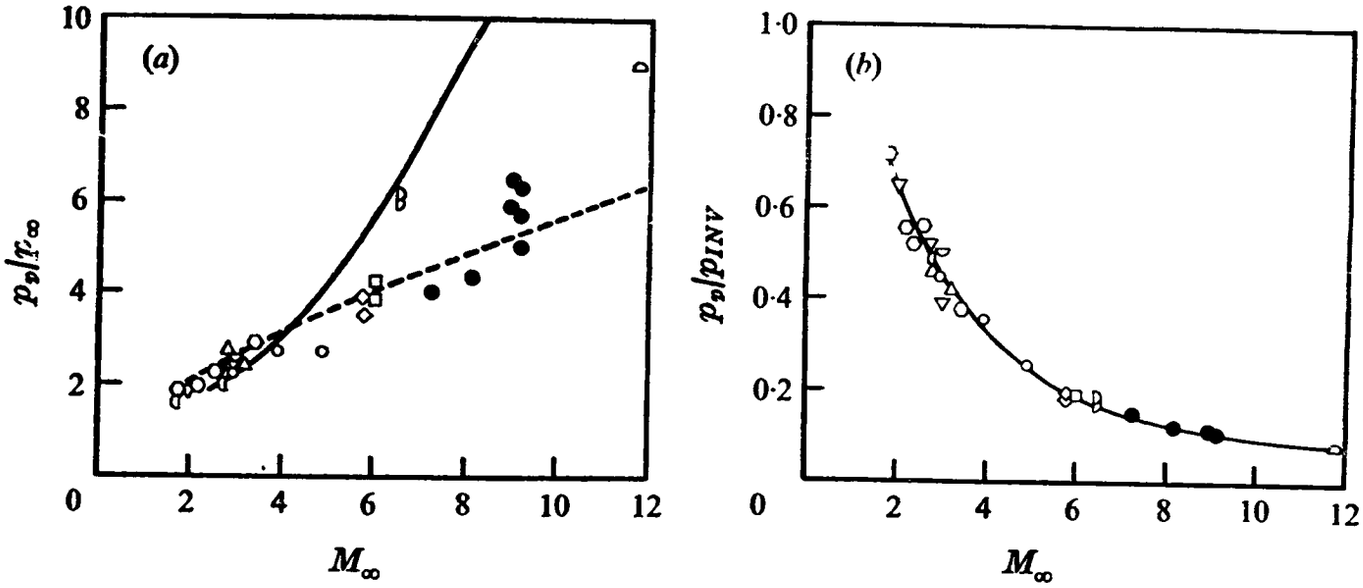

Figure 6. Correlation of Plateau Pressure Ahead of a Compression Corner, from Reference 15 as Collected in Reference 15, With Solid Points Due to Elfstrom

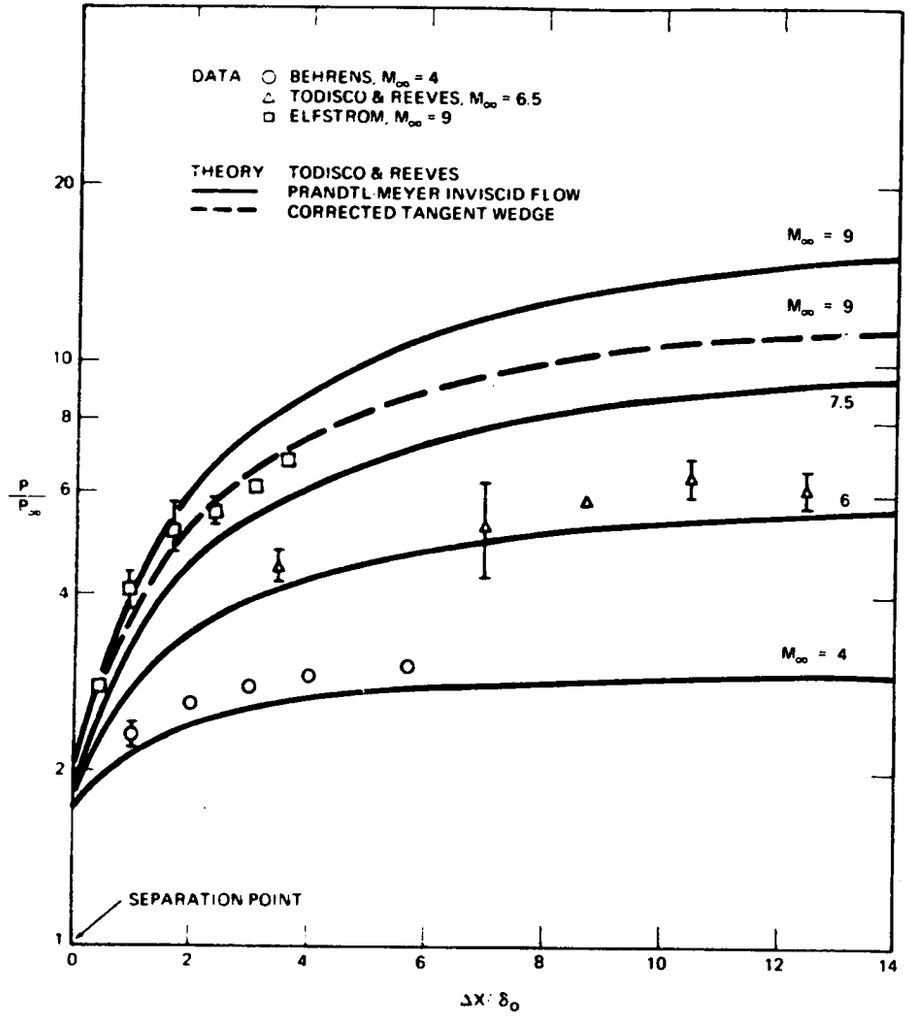

a) Pressure Distributions Downstream of Separation Point

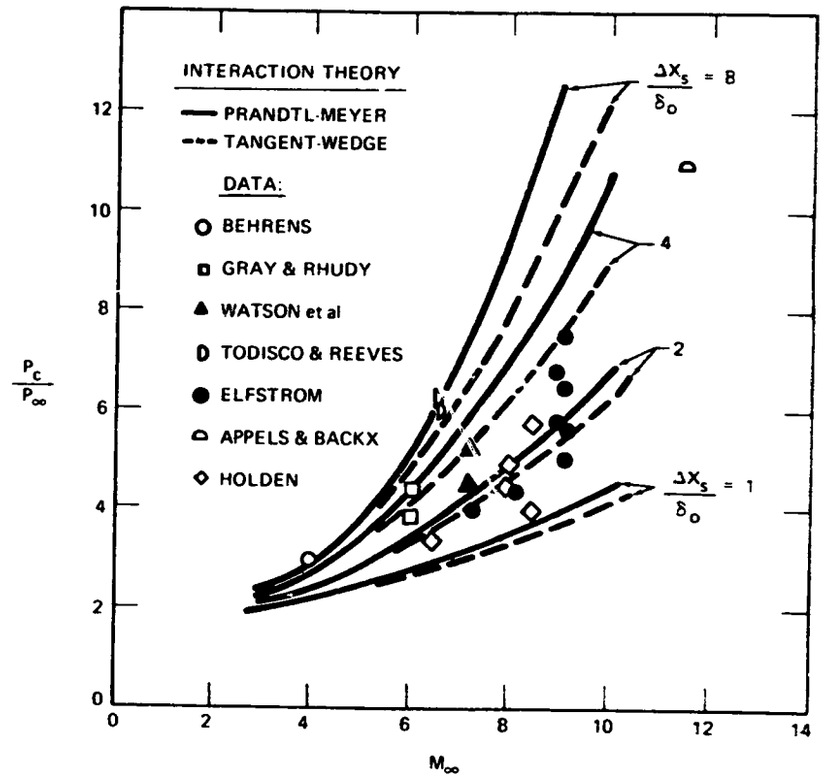

b) Variation of Pressure at Compression Corner with Length of Separation and M_∞

Figure 7. Correlation of Pressure Ahead of a Compression Corner, from Reference 16

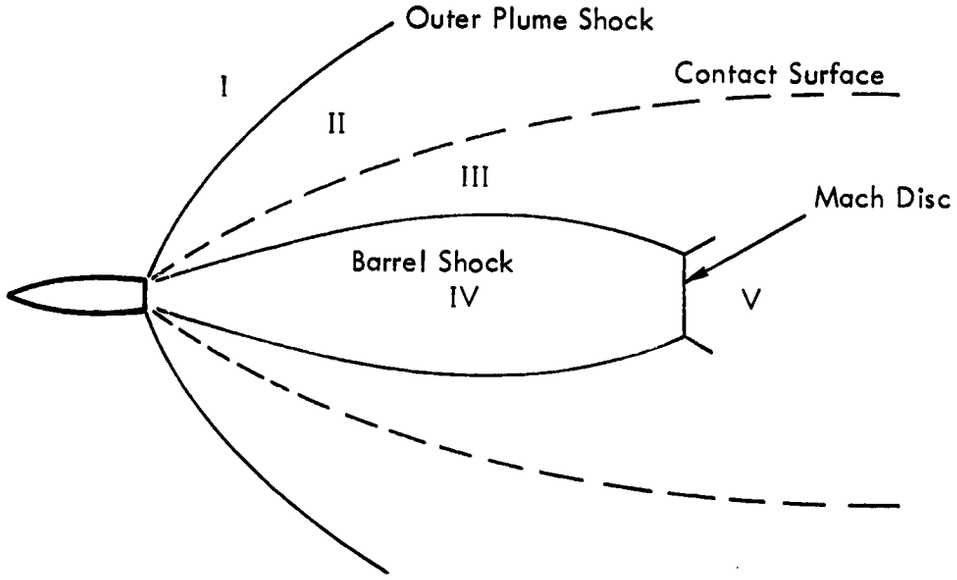

Figure 8. Inviscid High Speed Underexpanded Rocket Plume

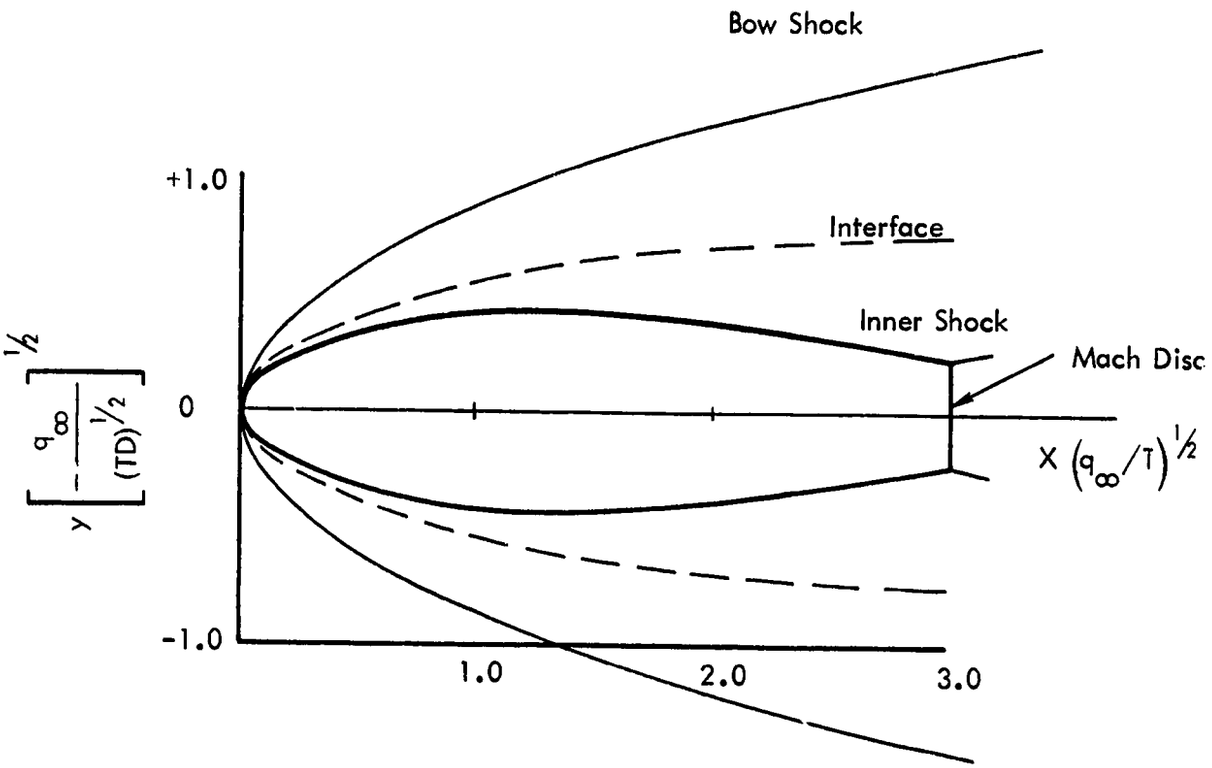

Figure 9. Universal Plume Shape, from Reference 25

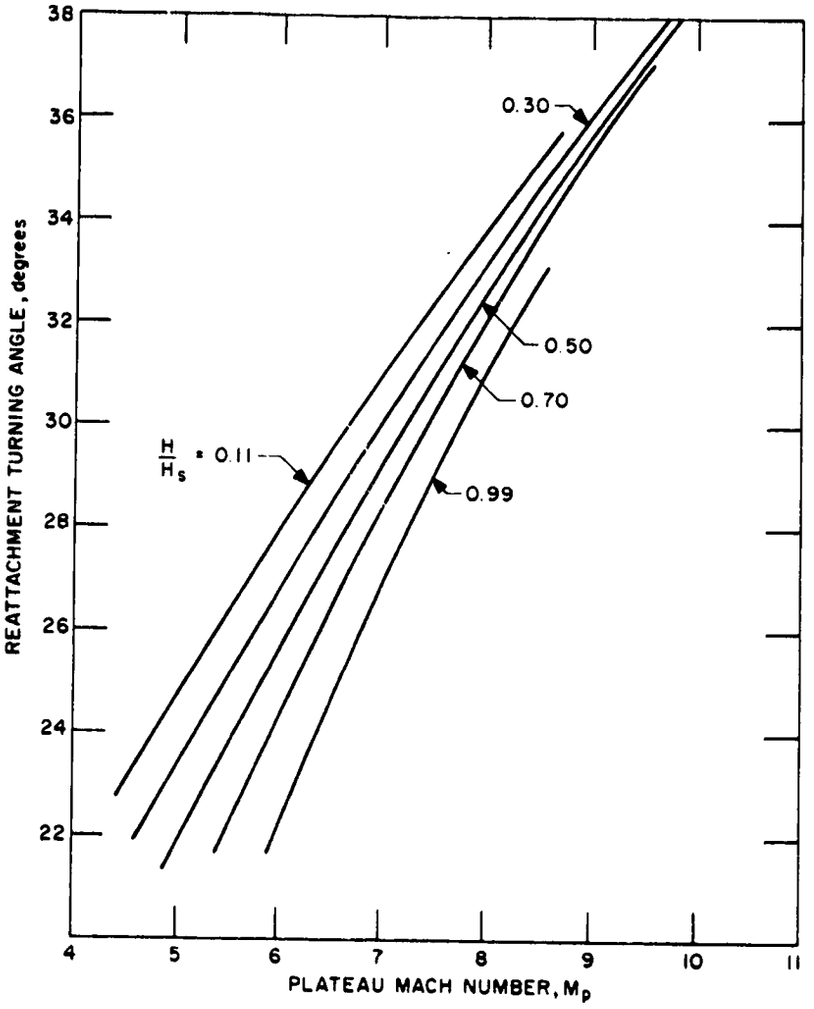

Figure 10. Turbulent Reattachment Solutions, from Reference 8

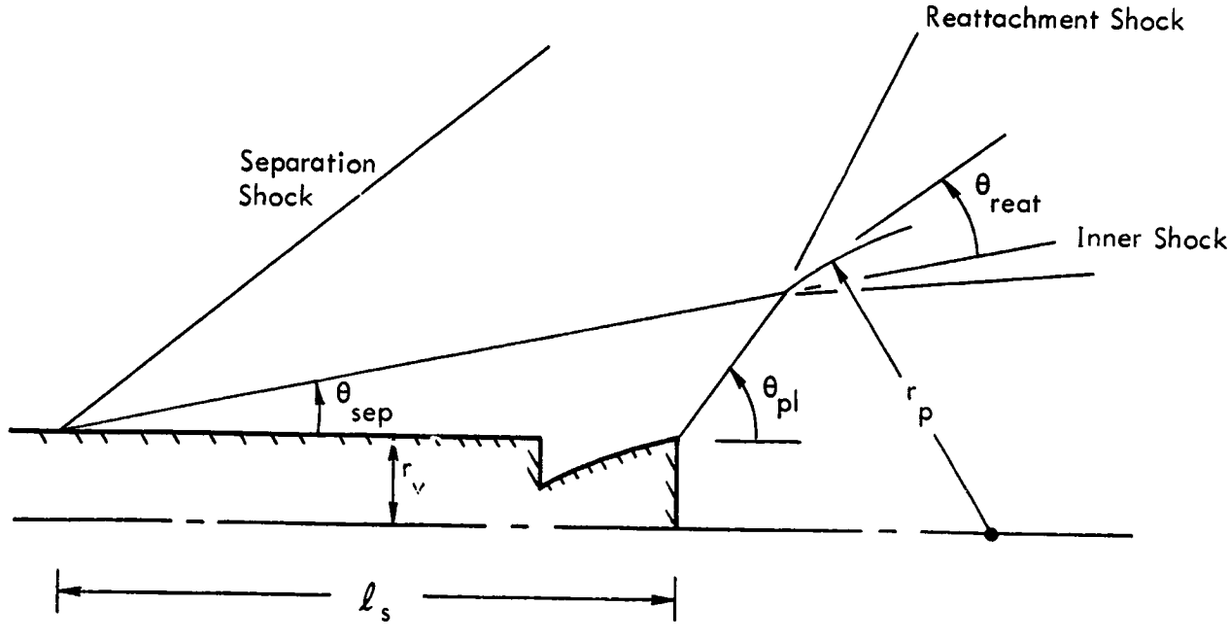

Figure 11. Geometry of Plume-Induced Separation Model

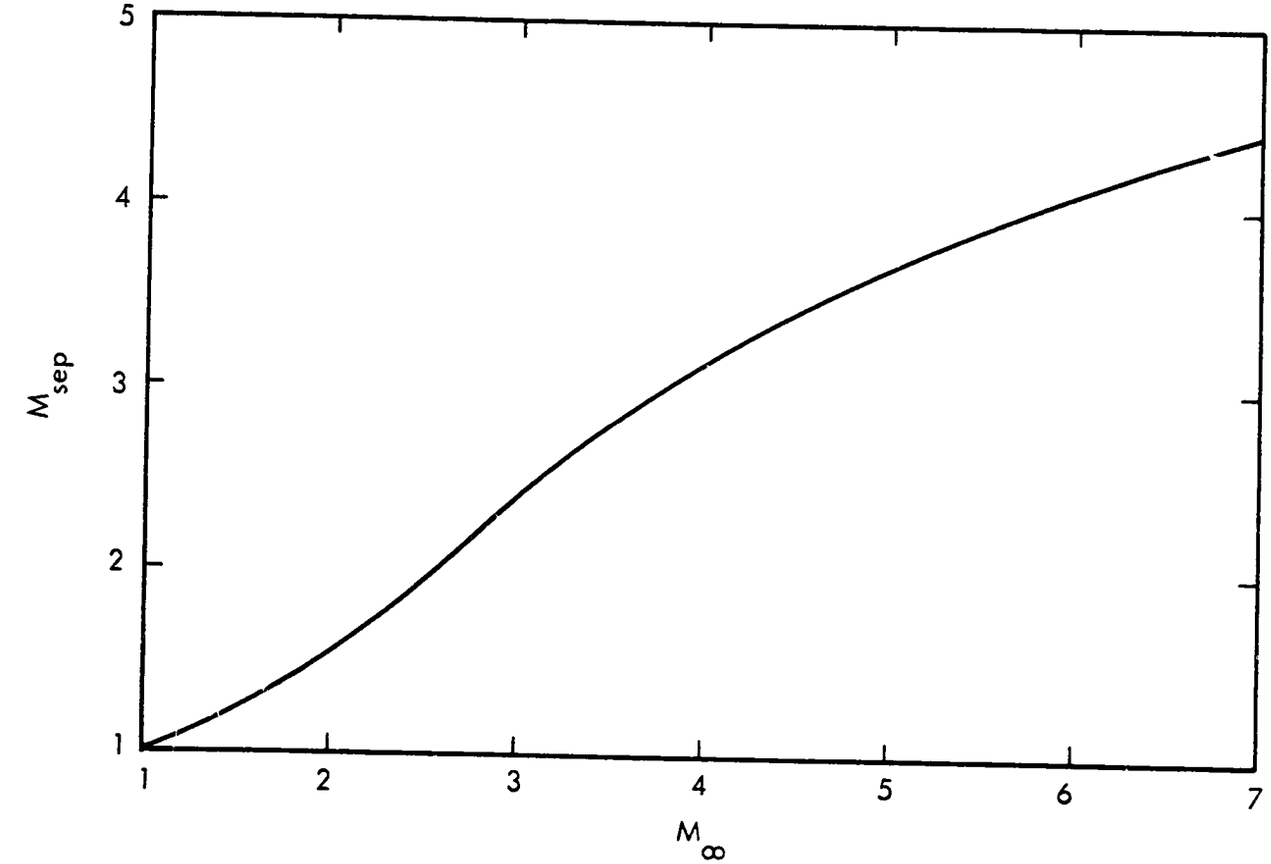

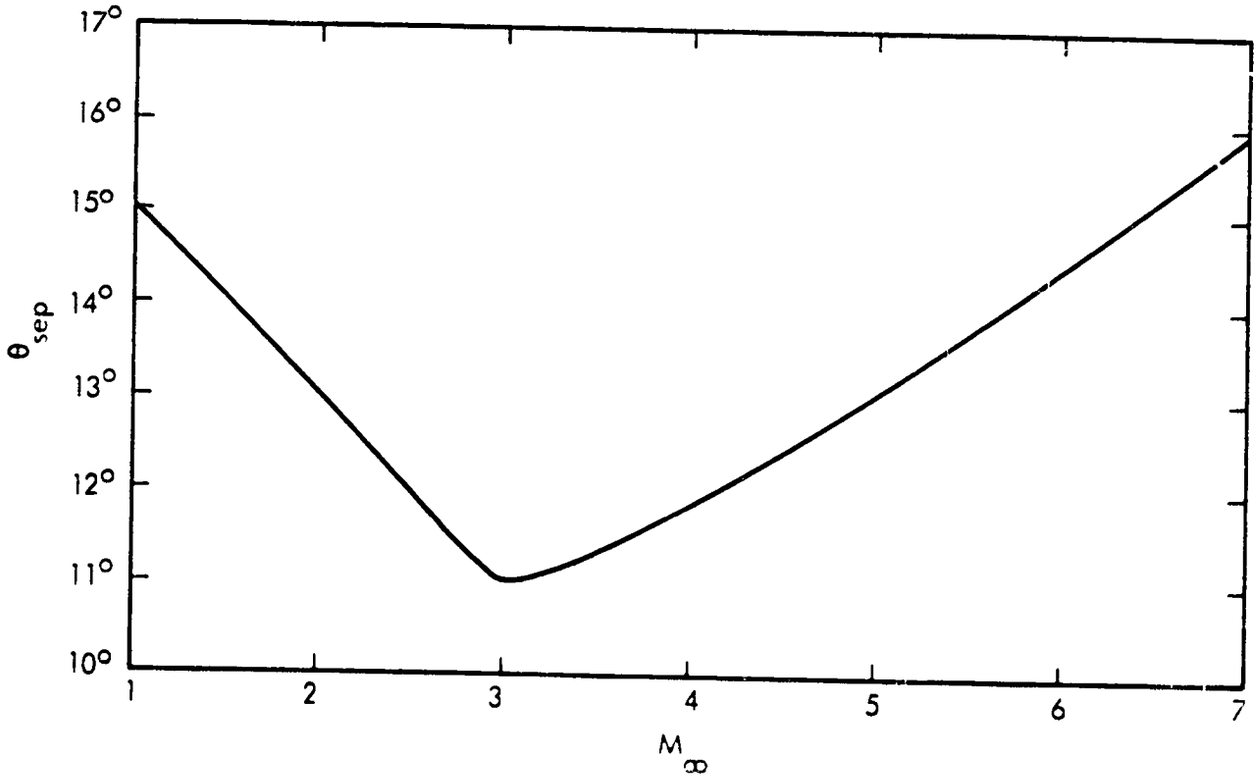

Figure 12. Separation Angle and Mach Number Used in Present Model

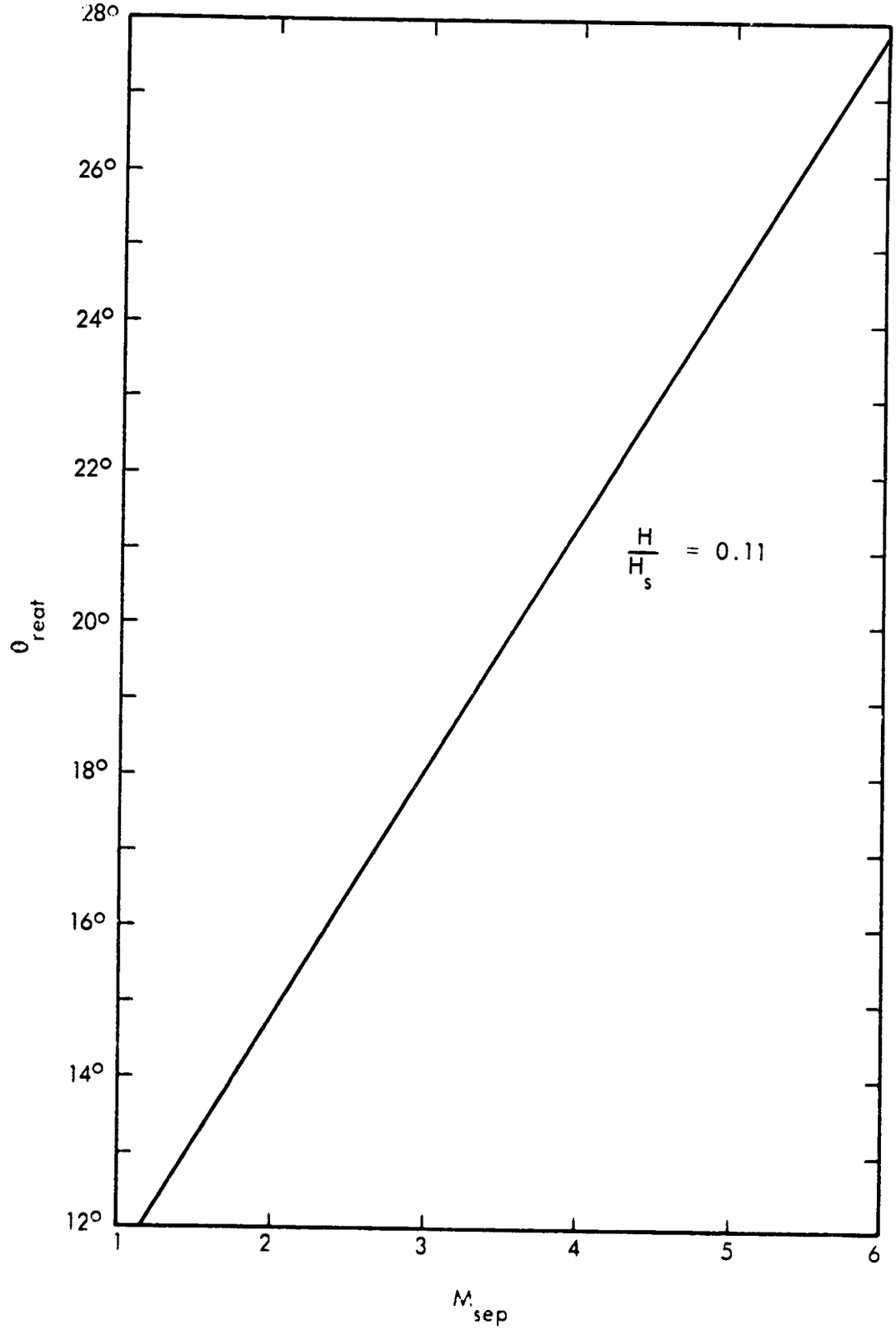

Figure 13. Reattachment Turning Angle vs Separation Mach Number Used in Present Model

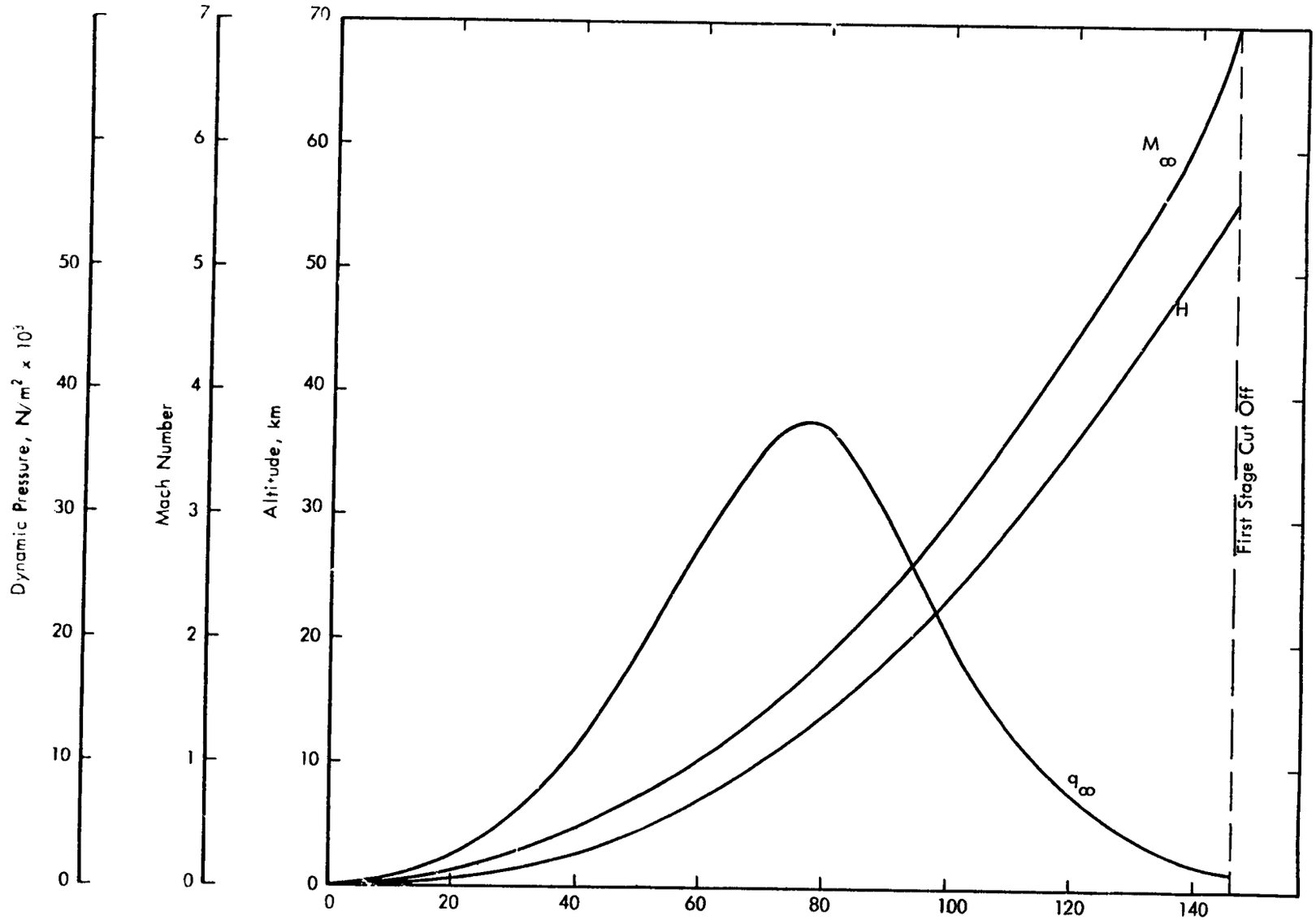

Figure 14. Nominal Apollo Trajectory, from Reference 28

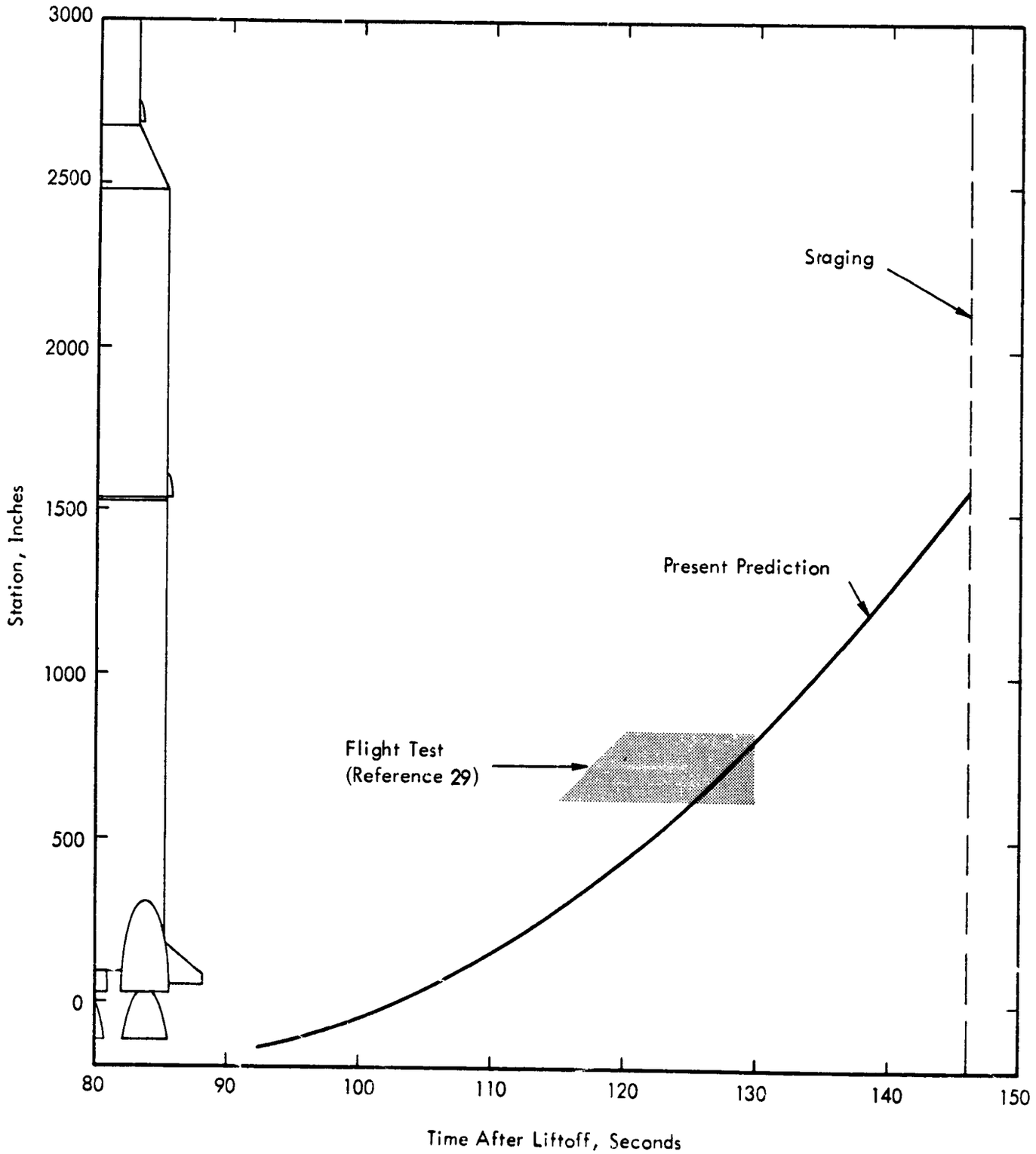

Figure 15. Prediction of Plume Induced-Separation Point on Saturn V, Apollo Trajectory

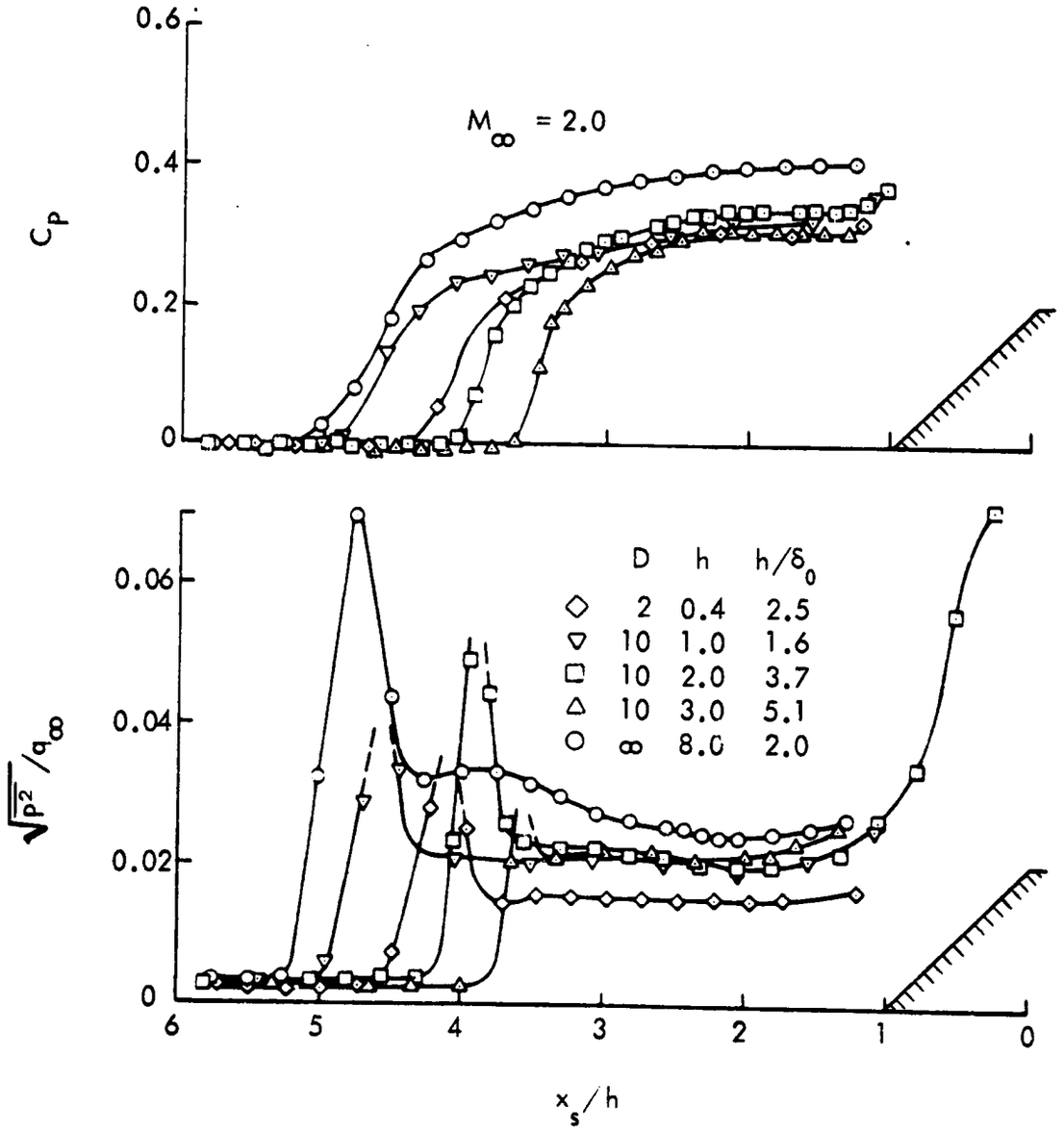

Figure 16. Longitudinal Distributions of Steady and Fluctuating Pressure Ahead of a Compression Corner, from Reference 30

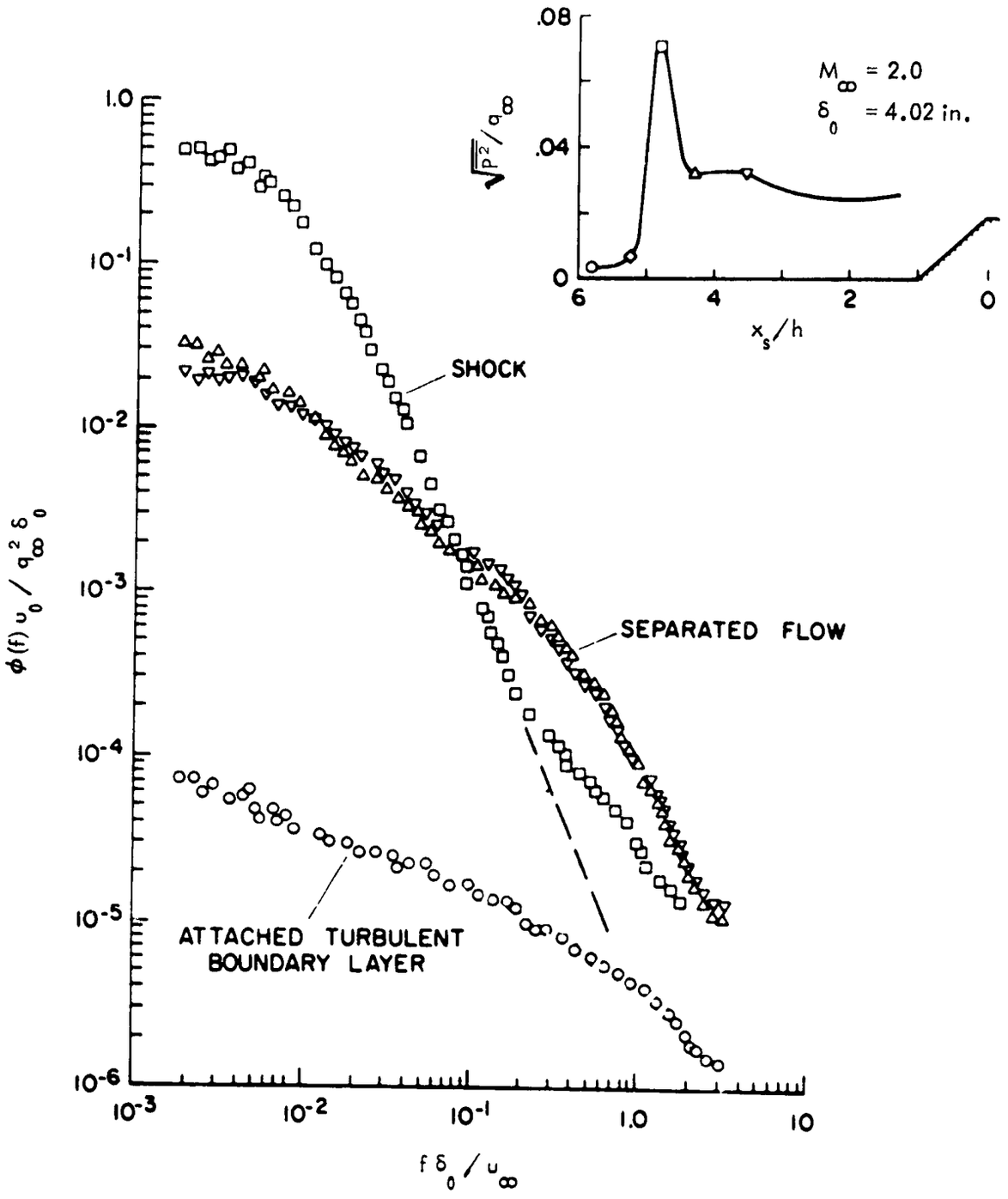

○ Attached turbulent boundary layer

▽ △ Non-homogeneous separated flow

□ Shock wave oscillation

--- Extrapolated shock oscillation alone

Figure 17. Typical Power Spectra in Region Ahead of a Supersonic Compression Corner, from Reference 30

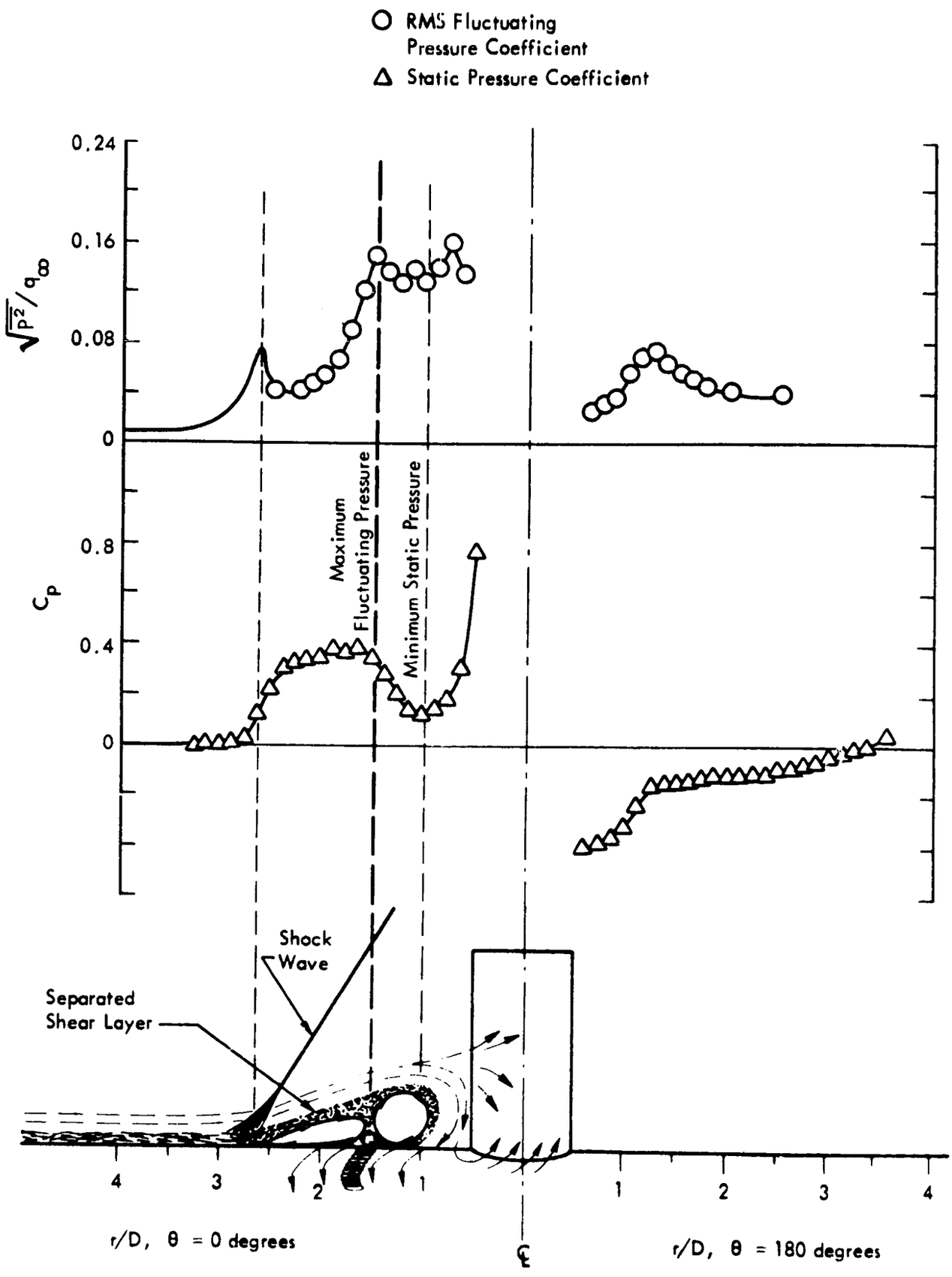

Figure 18. Static and Fluctuating Pressure Distribution Ahead of a Three-Dimensional Protuberance, Showing Multiple Eddy Structure in Separation Region

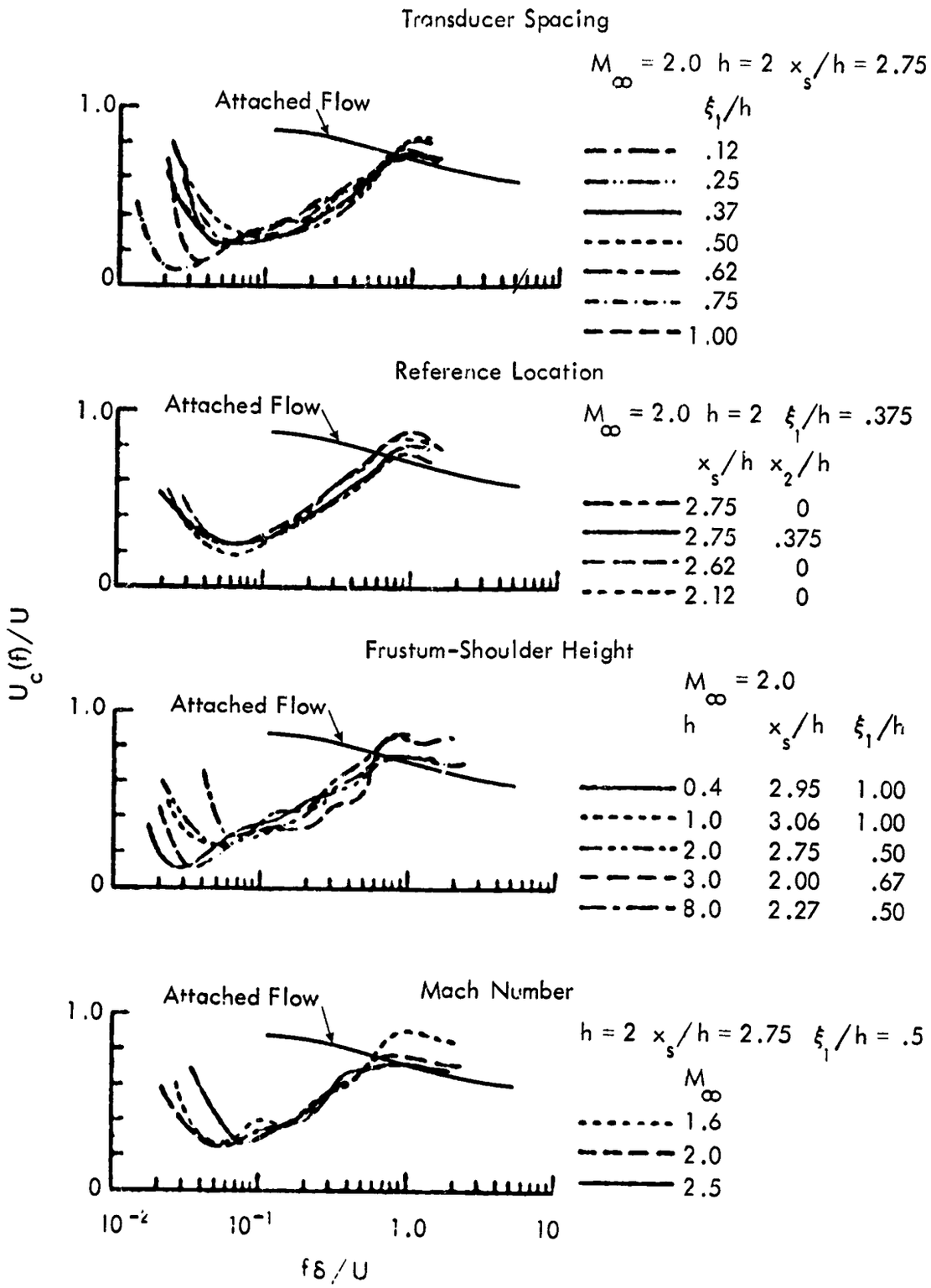

Figure 19. Narrow-Band Convection Velocities in Separated Region, from Reference 30. Attached Flow from Reference 33

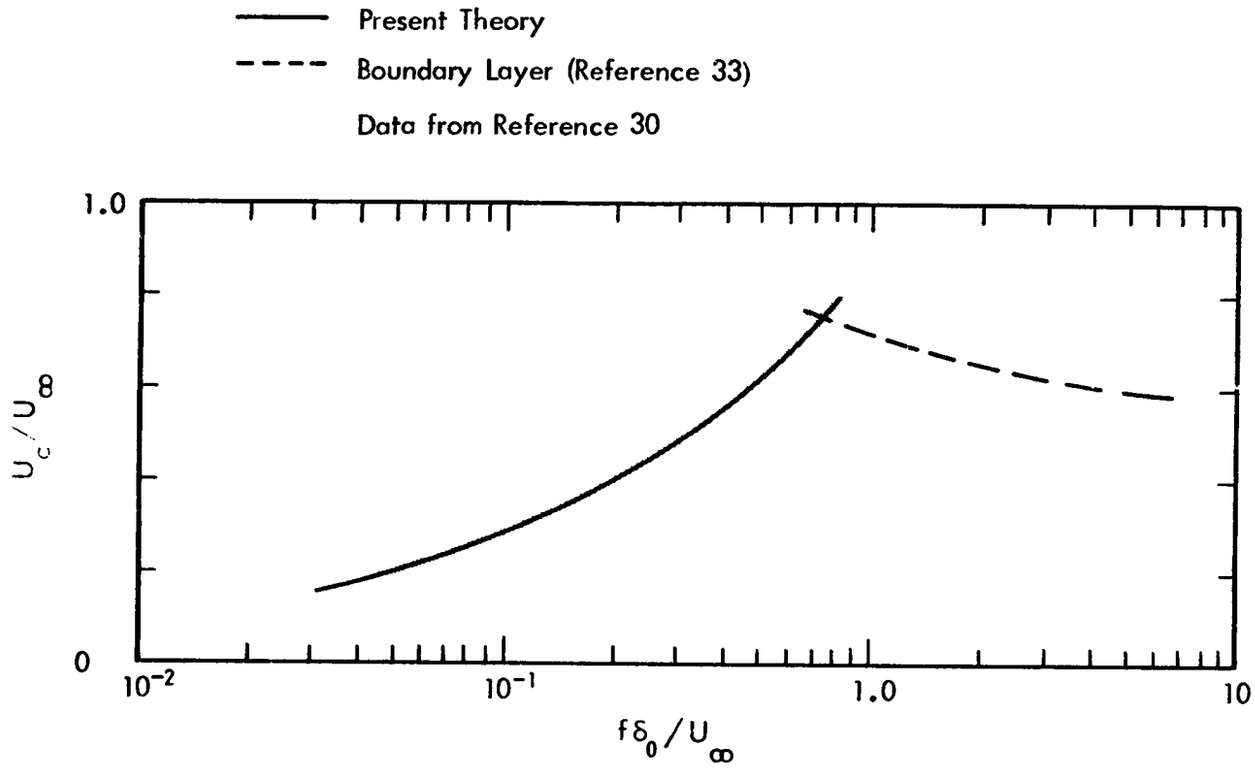

Figure 20. Comparison of Present Entrainment Model for Convection Speed with Data of Reference 30

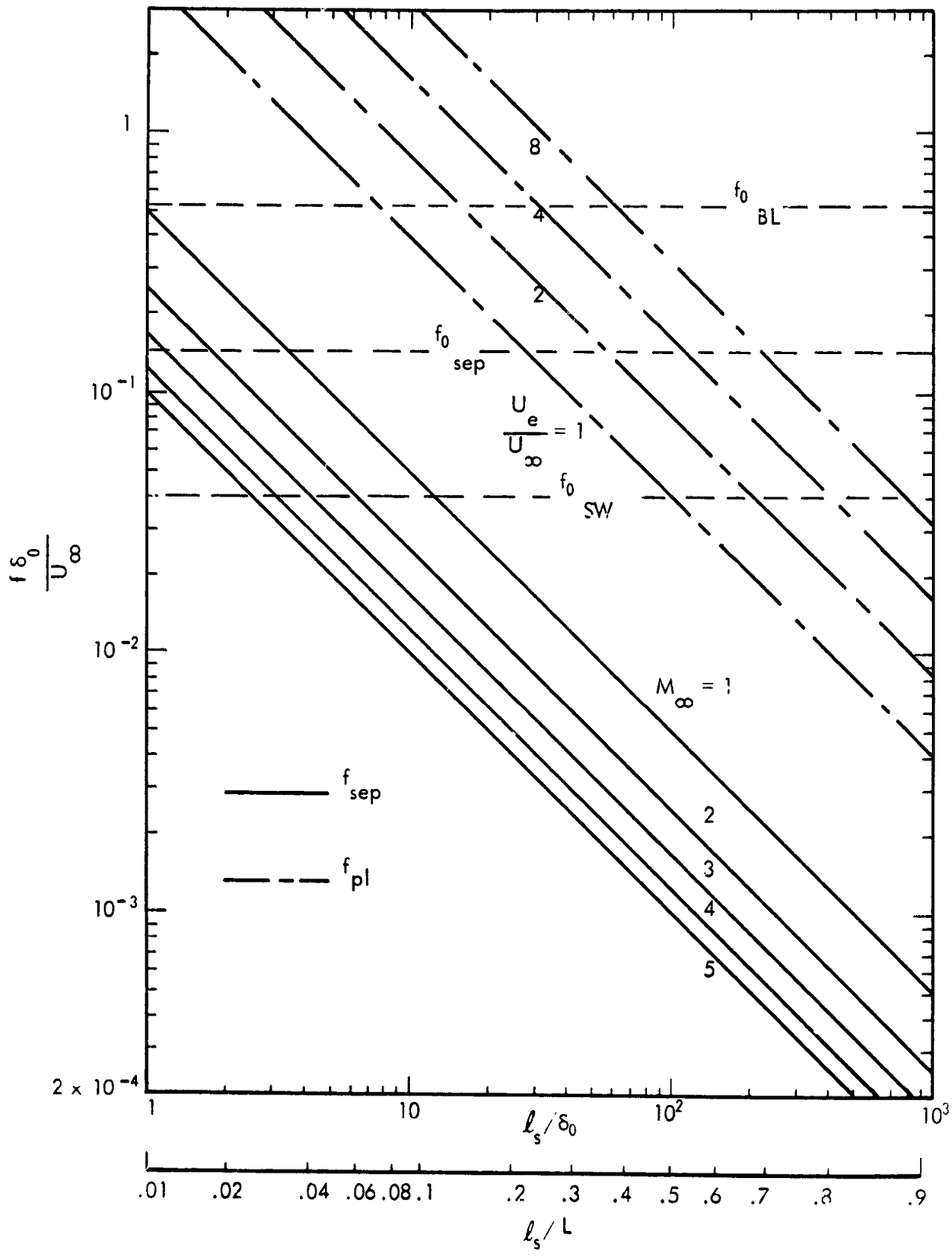

Figure 21. Comparison of Characteristic Frequencies of Separated Flow and Plume Flow

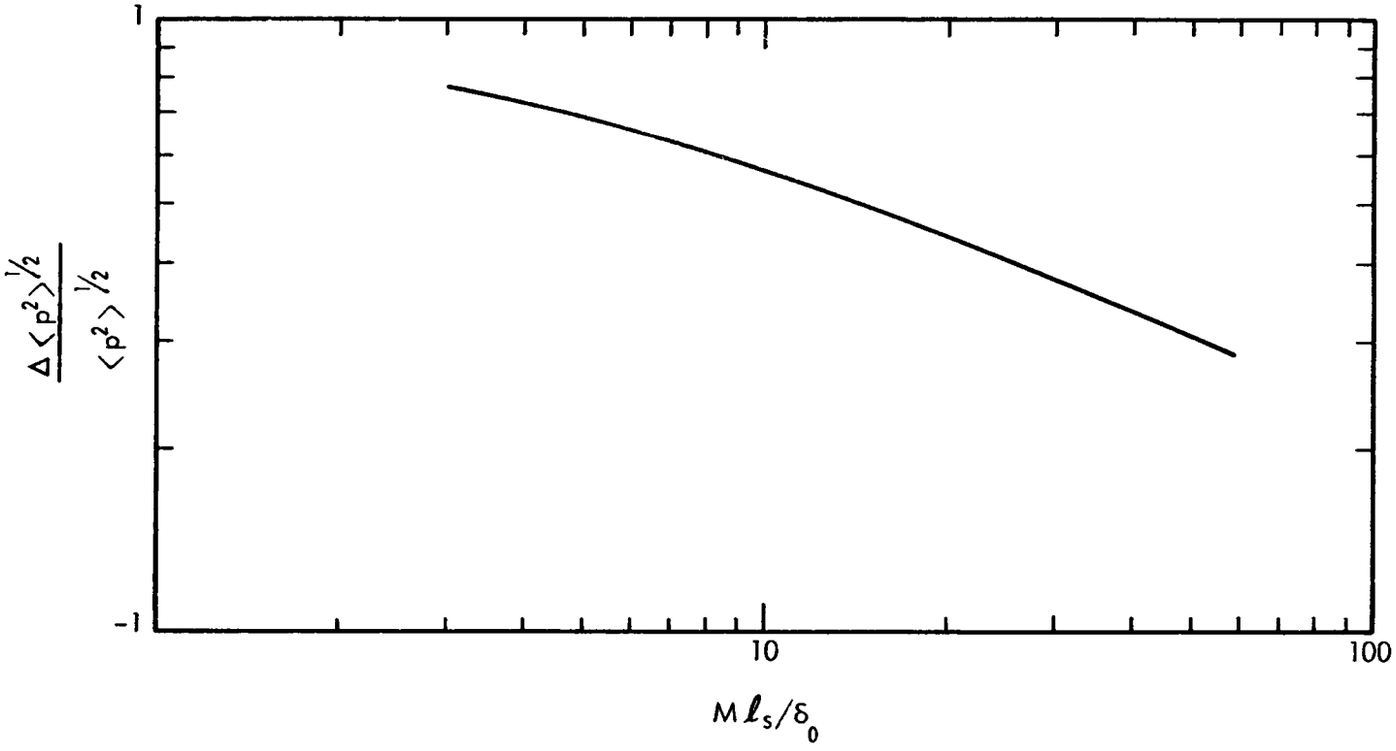

Figure 22. Fraction of Separation Region Fluctuating Pressure Which Can Couple to Plume Motion

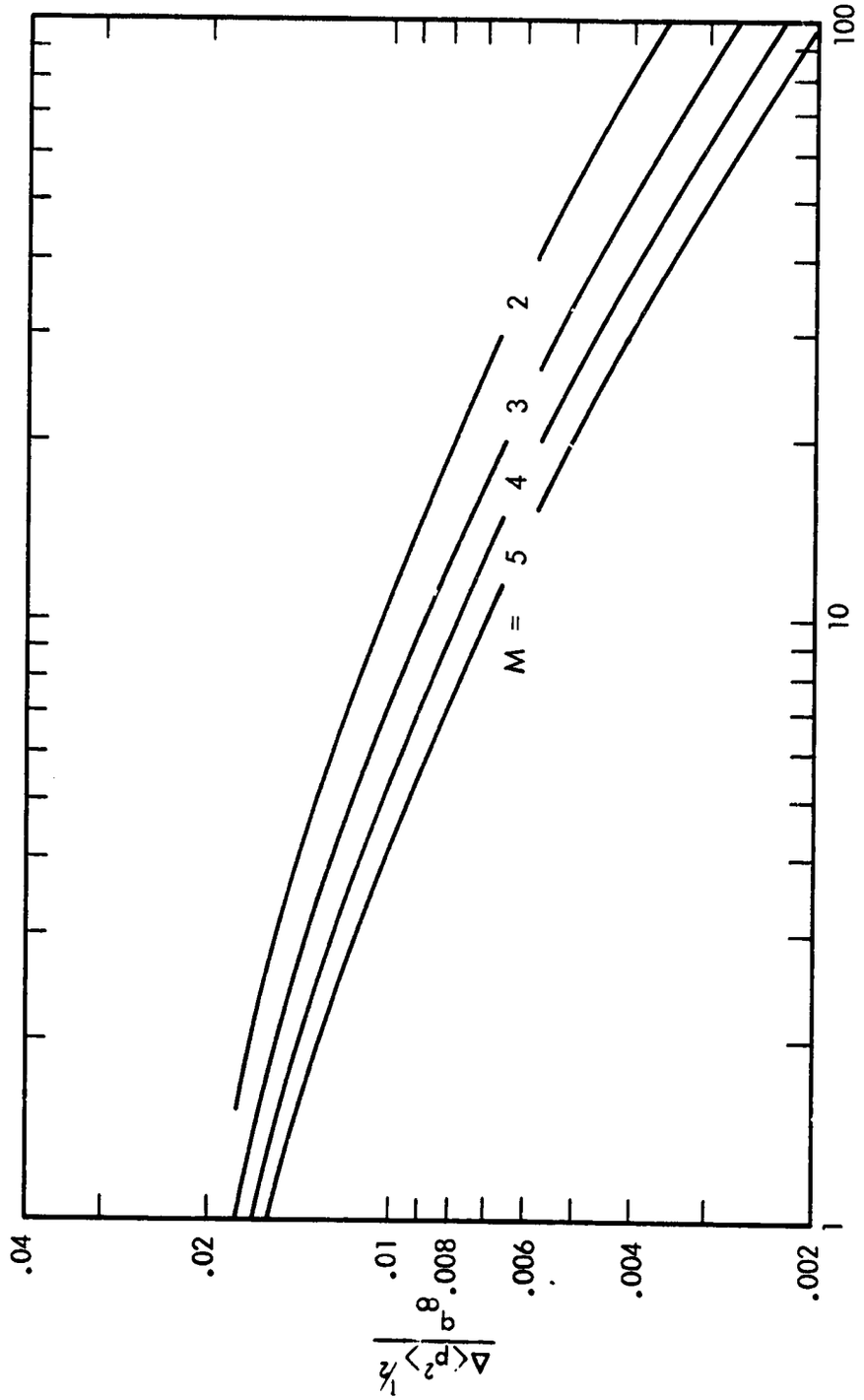

Figure 23. Feedback Pressure Coefficient Versus Separation Length

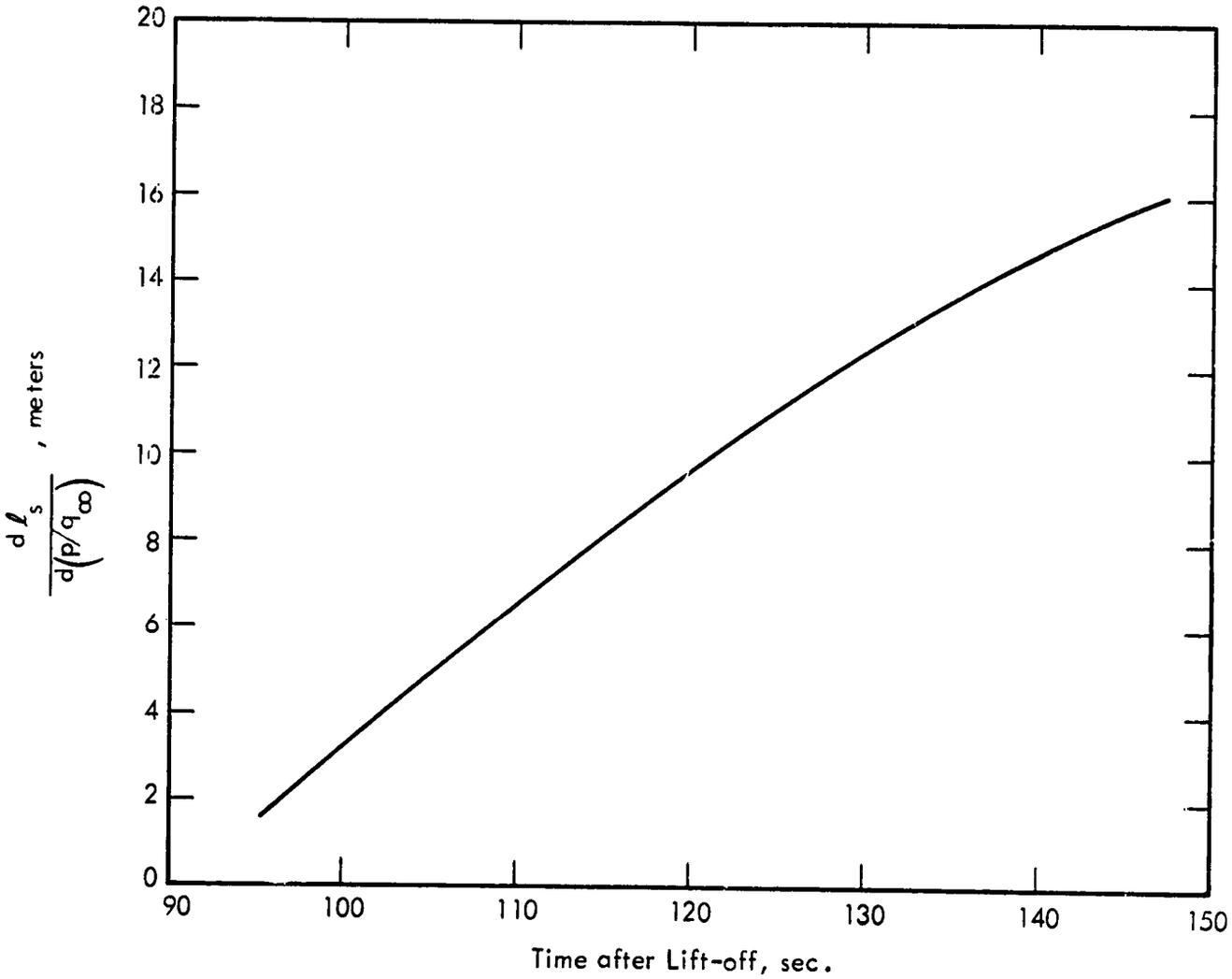

Figure 24. Change in Separation Length with Change in Plateau Pressure, for Saturn V

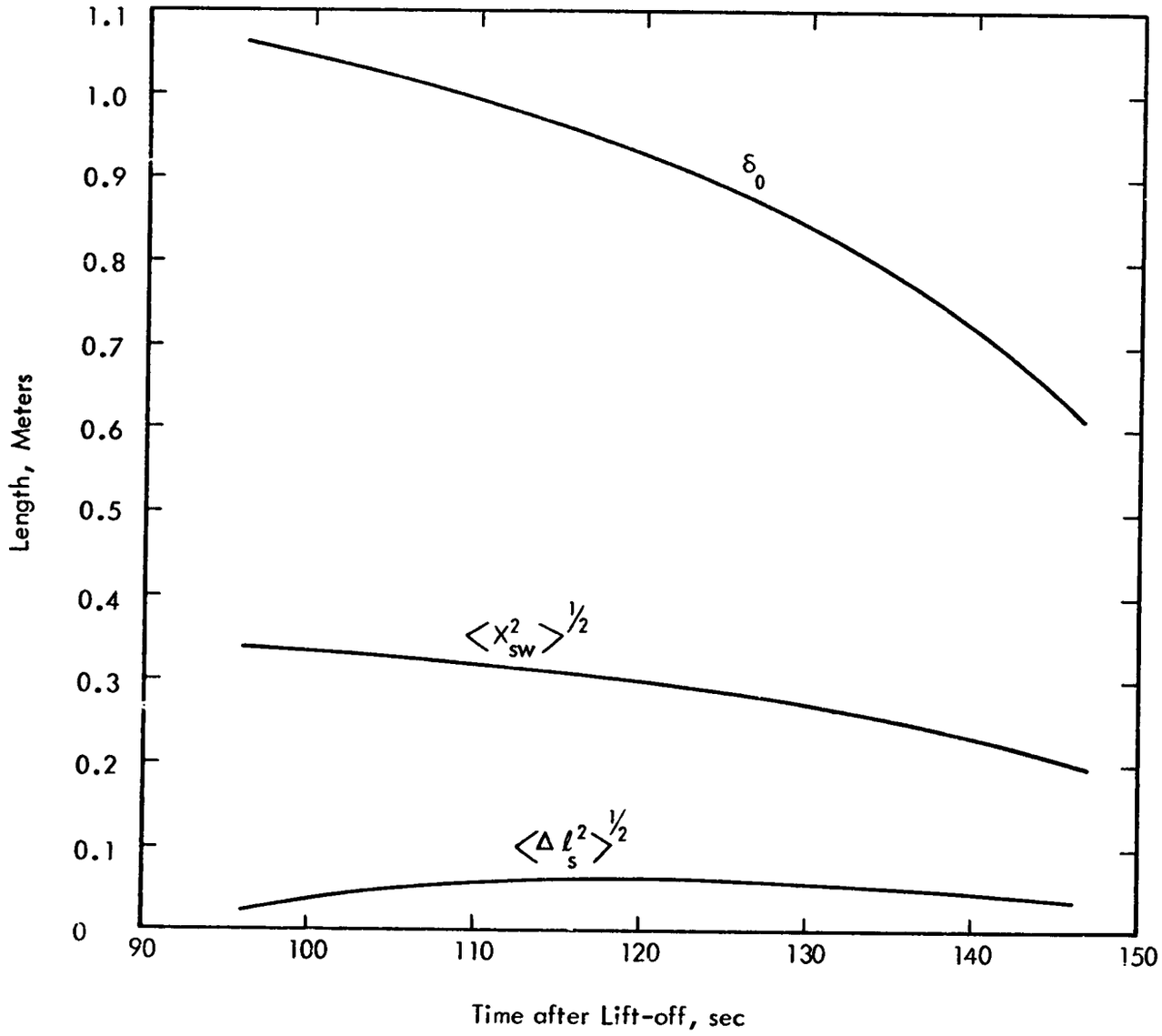

Figure 25. Separation Length Fluctuation, Boundary Layer Thickness at Separation, and Shock Oscillation Distance for Equivalent Rigid Flare, for Saturn V

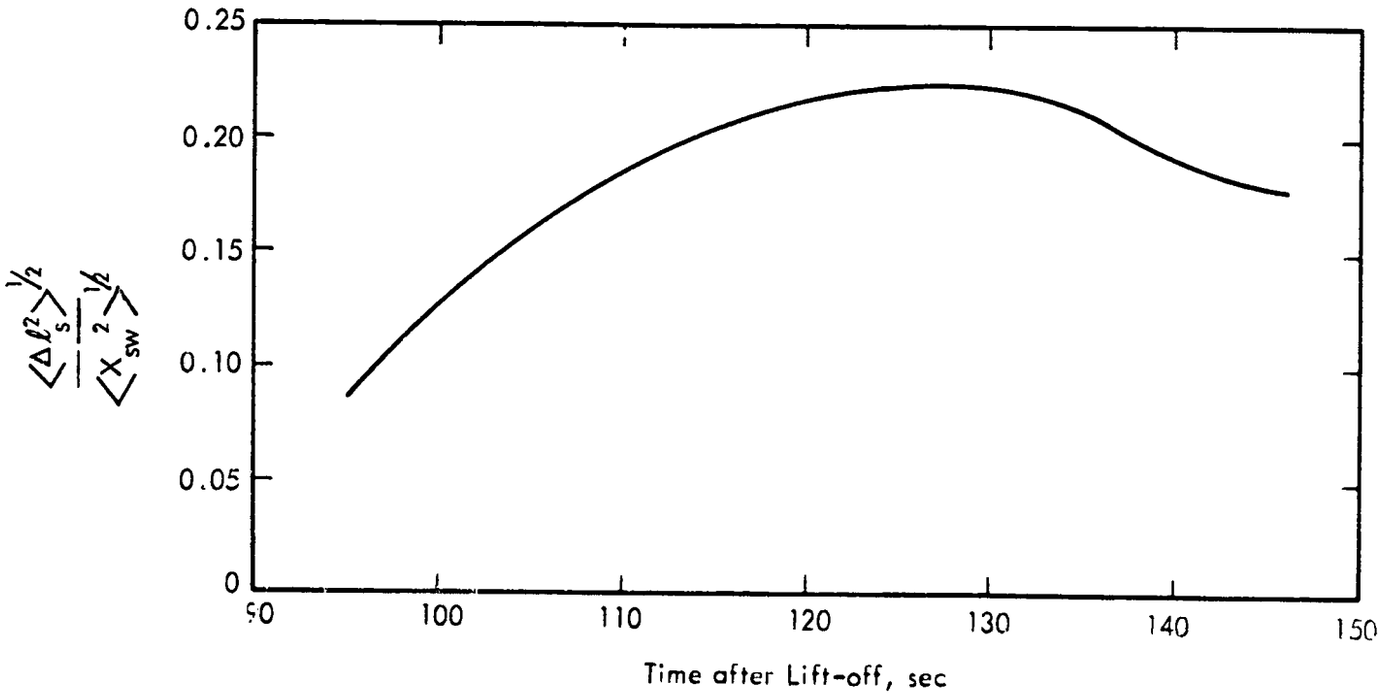

Figure 26. Root Mean Square Fluctuation of Separation Length for Plume, Normalized by Root Mean Square Shock Displacement for Rigid Flare. Saturn V, Apollo Trajectory

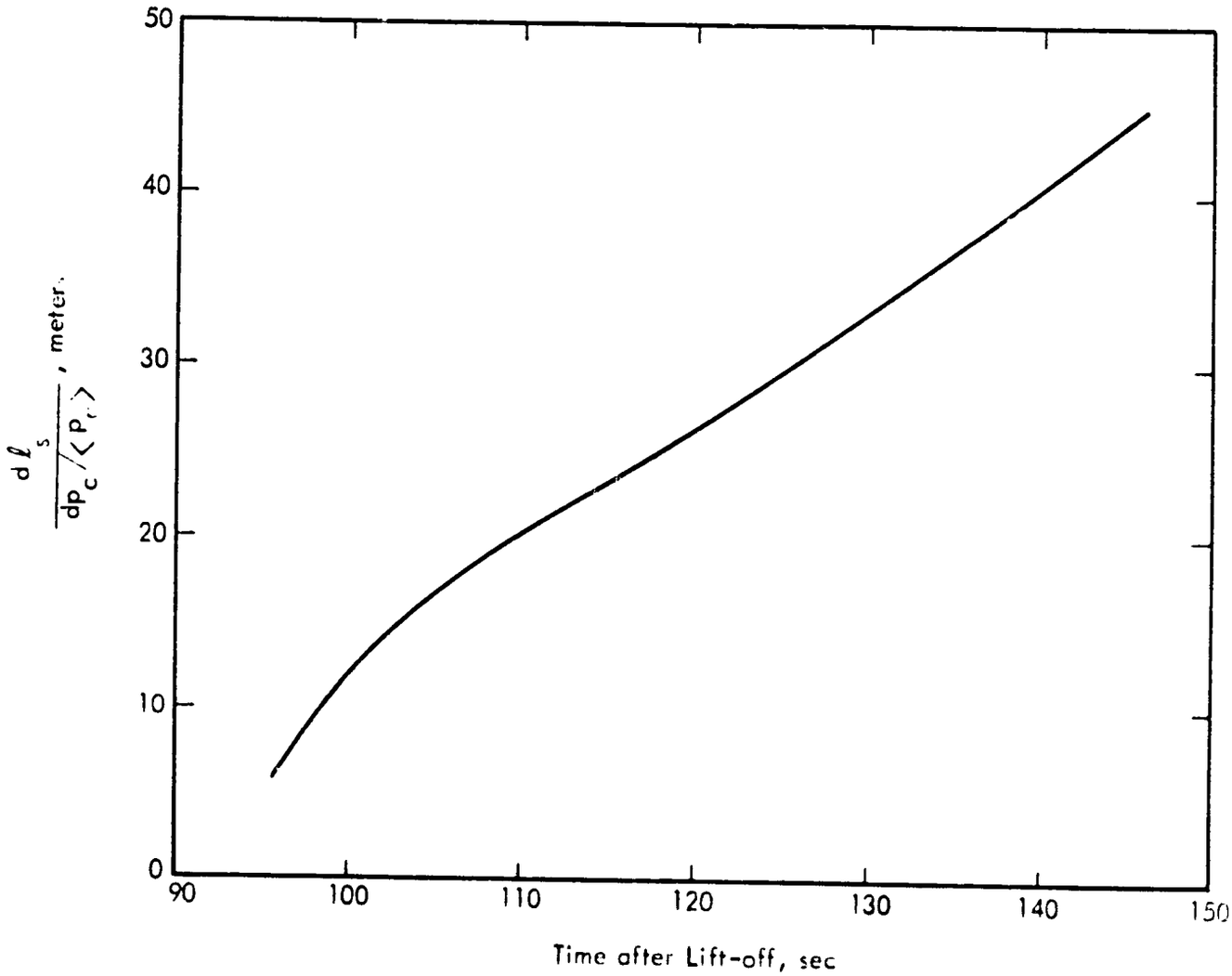

Figure 27. Change of Separation Length with Change in Chamber Pressure, for Saturn V

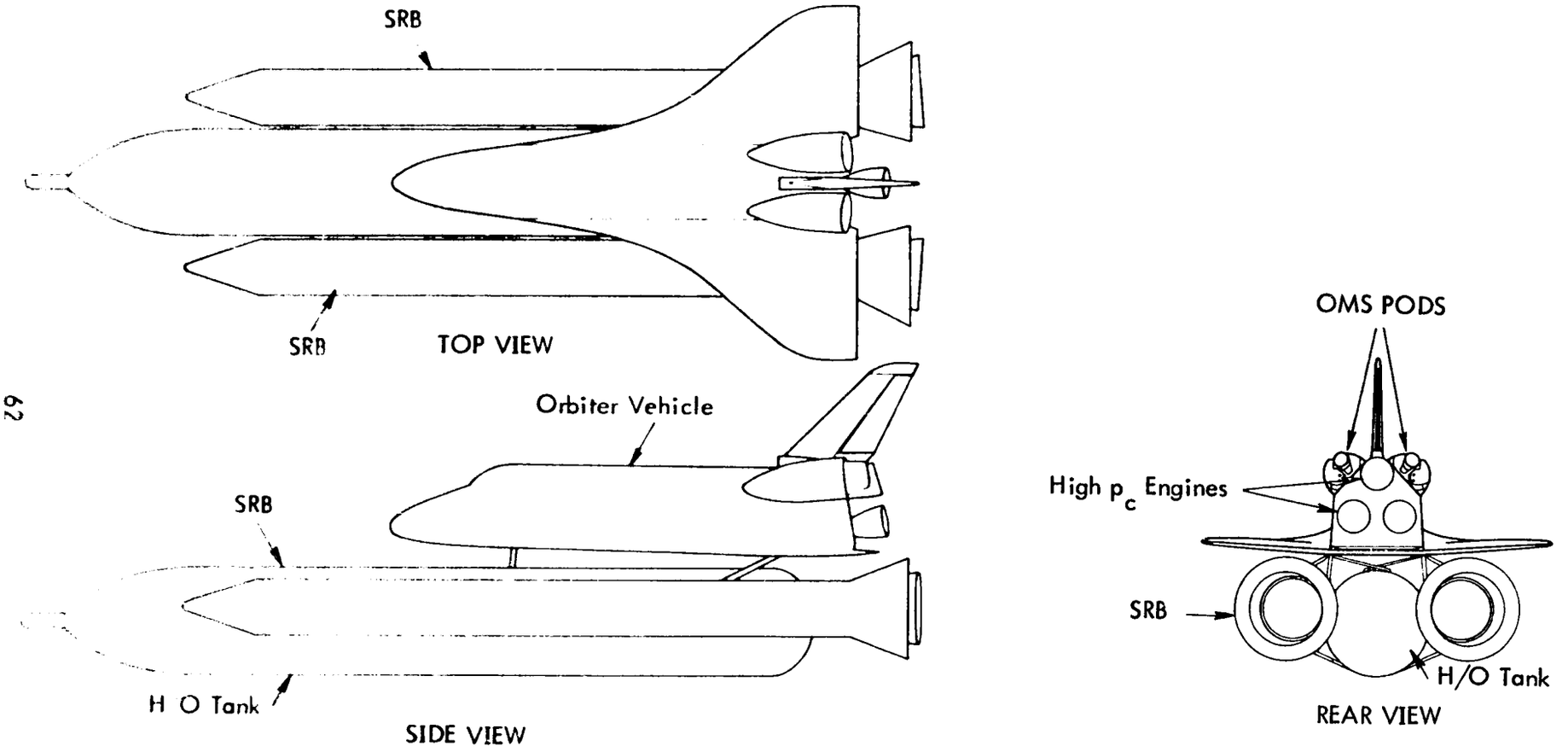

Figure 28. Schematic of PRR Parallel-Burn Space Shuttle Launch Configuration

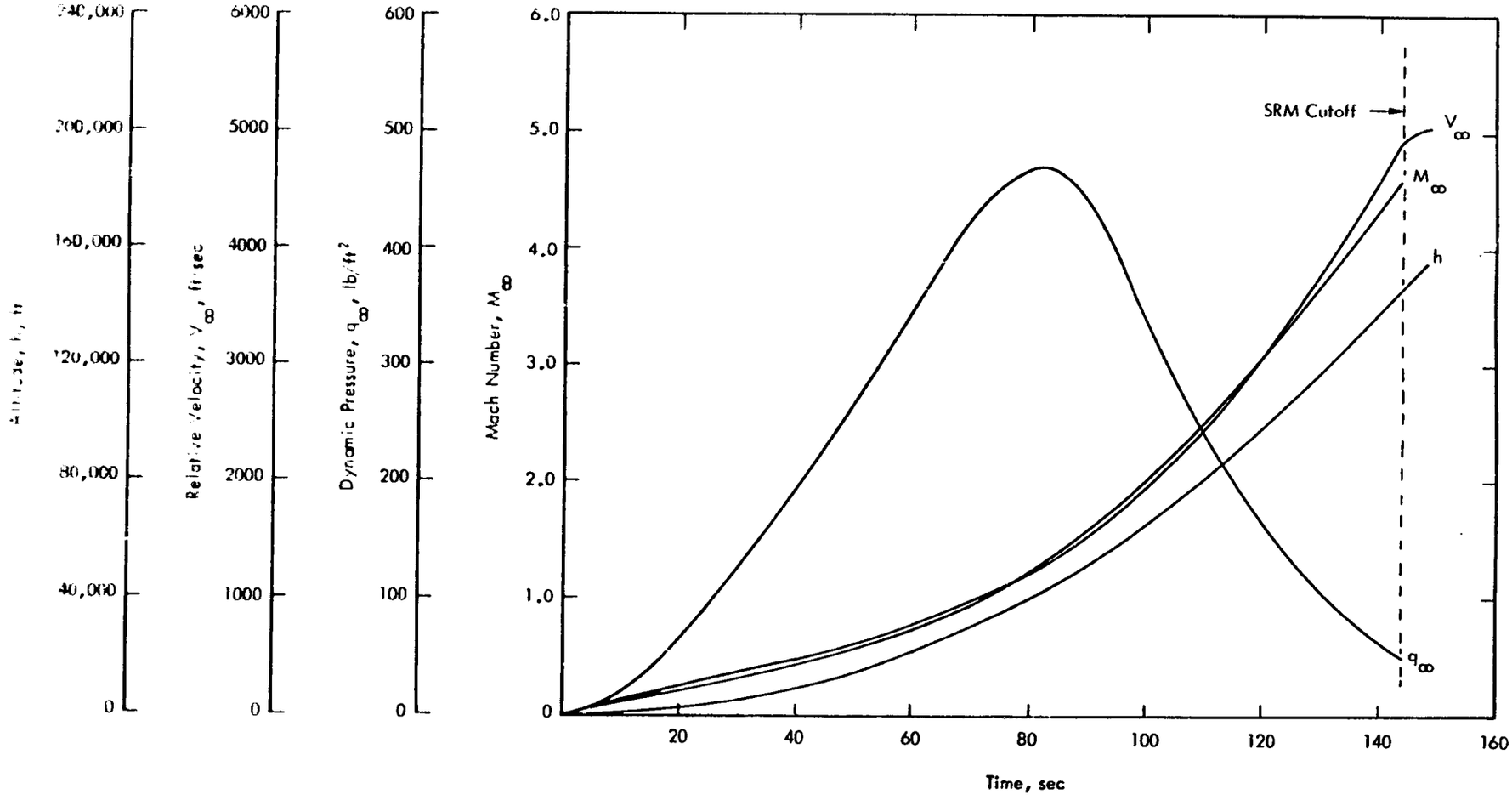

Figure 29. Trajectory Parameters for Due East Mission

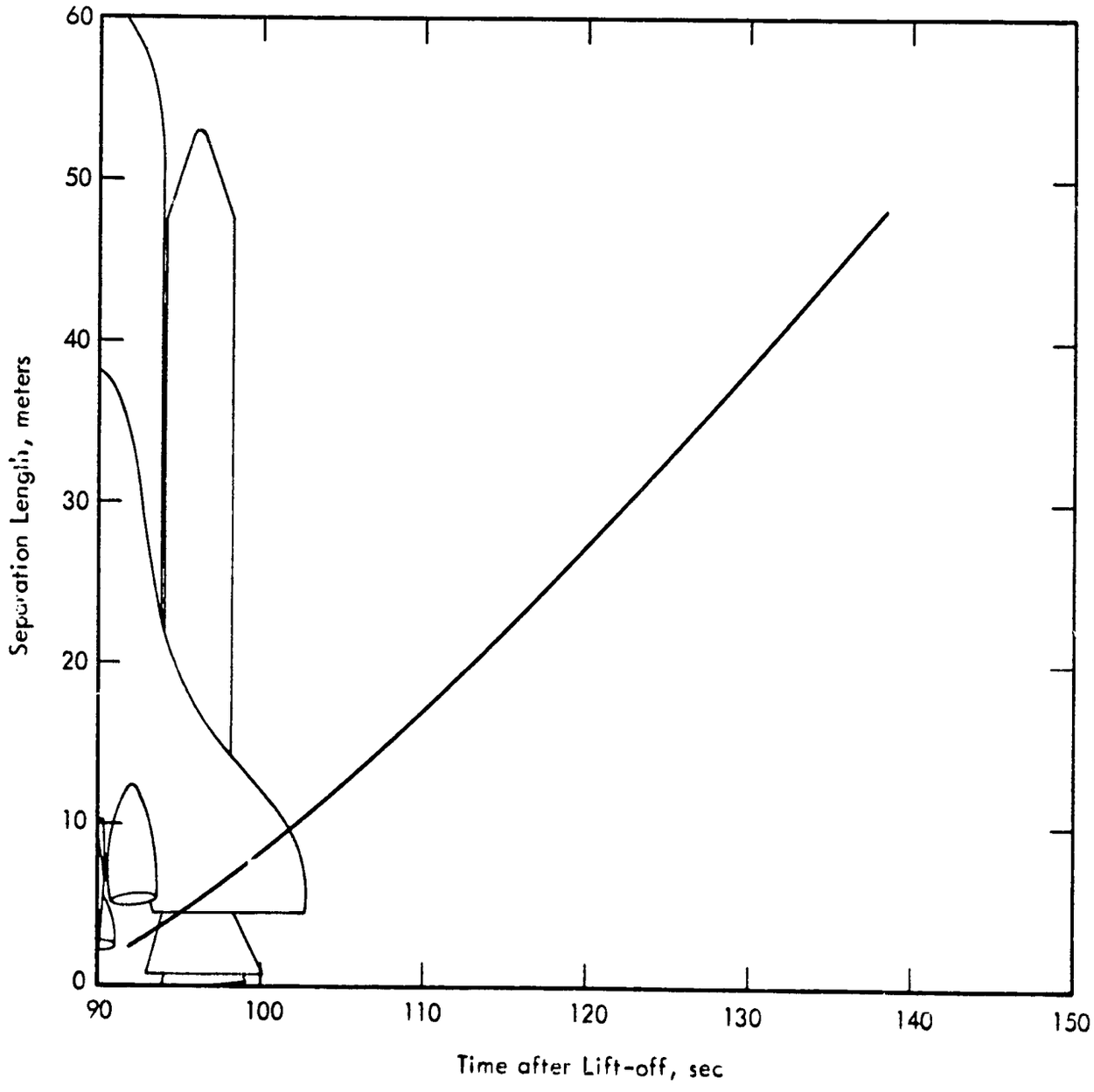

Figure 30. Prediction of Plume-Induced Separation Point on Shuttle SRB

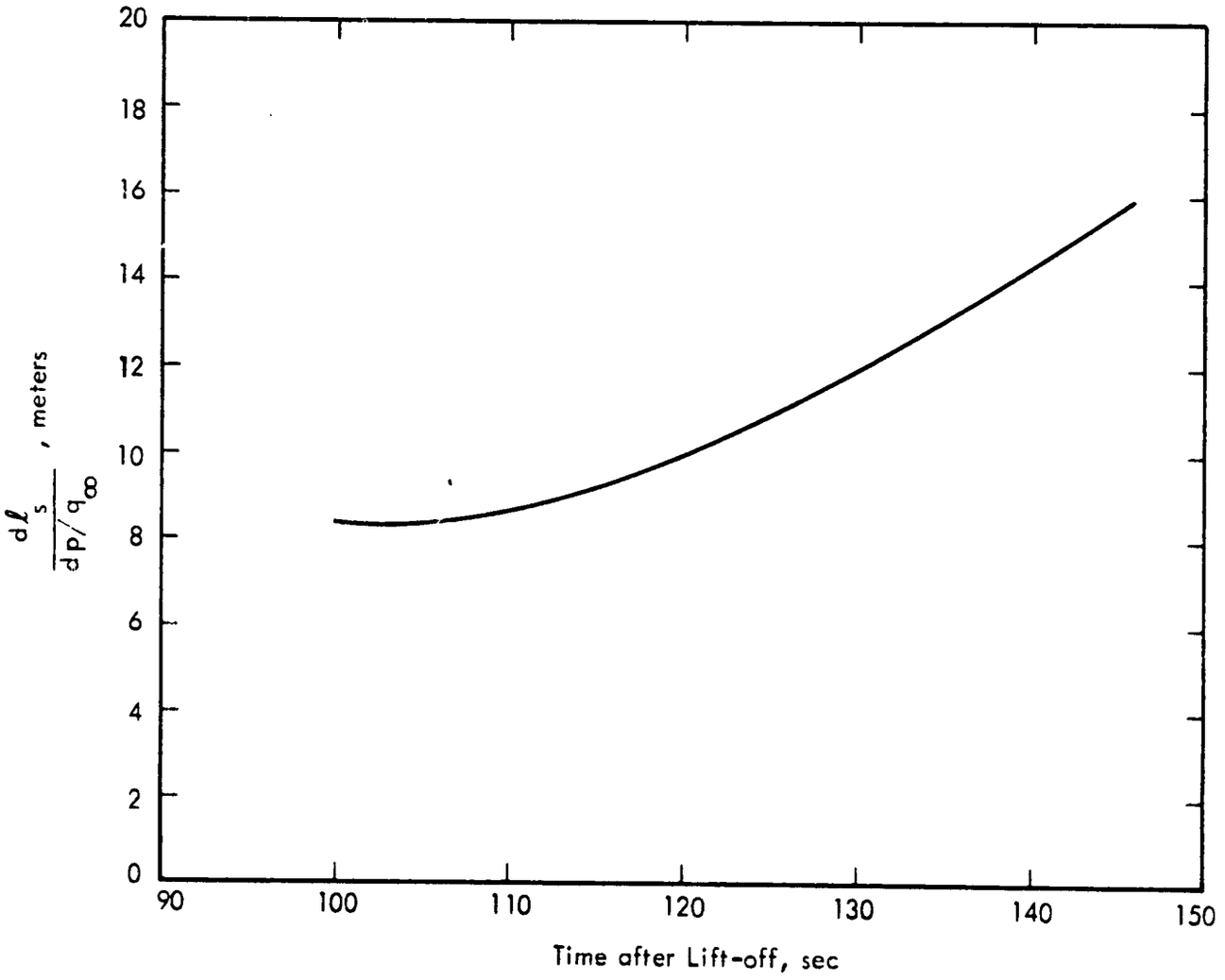

Figure 31. Change in Separation Length with Change in Plateau Pressure for Shuttle SRB

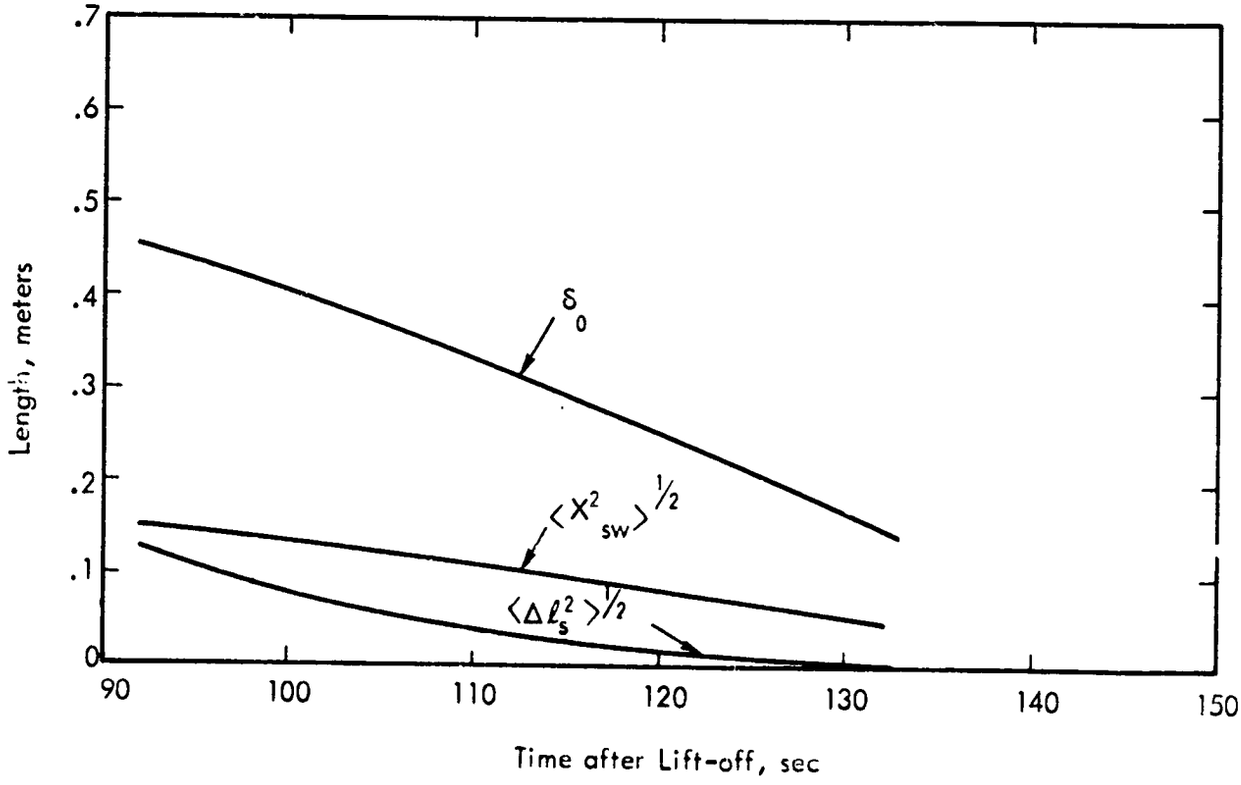

Figure 32. Separation Length Fluctuation, Boundary Layer Thickness at Separation, and Shock Oscillation Distance for Equivalent Rigid Flare, for Shuttle SRB

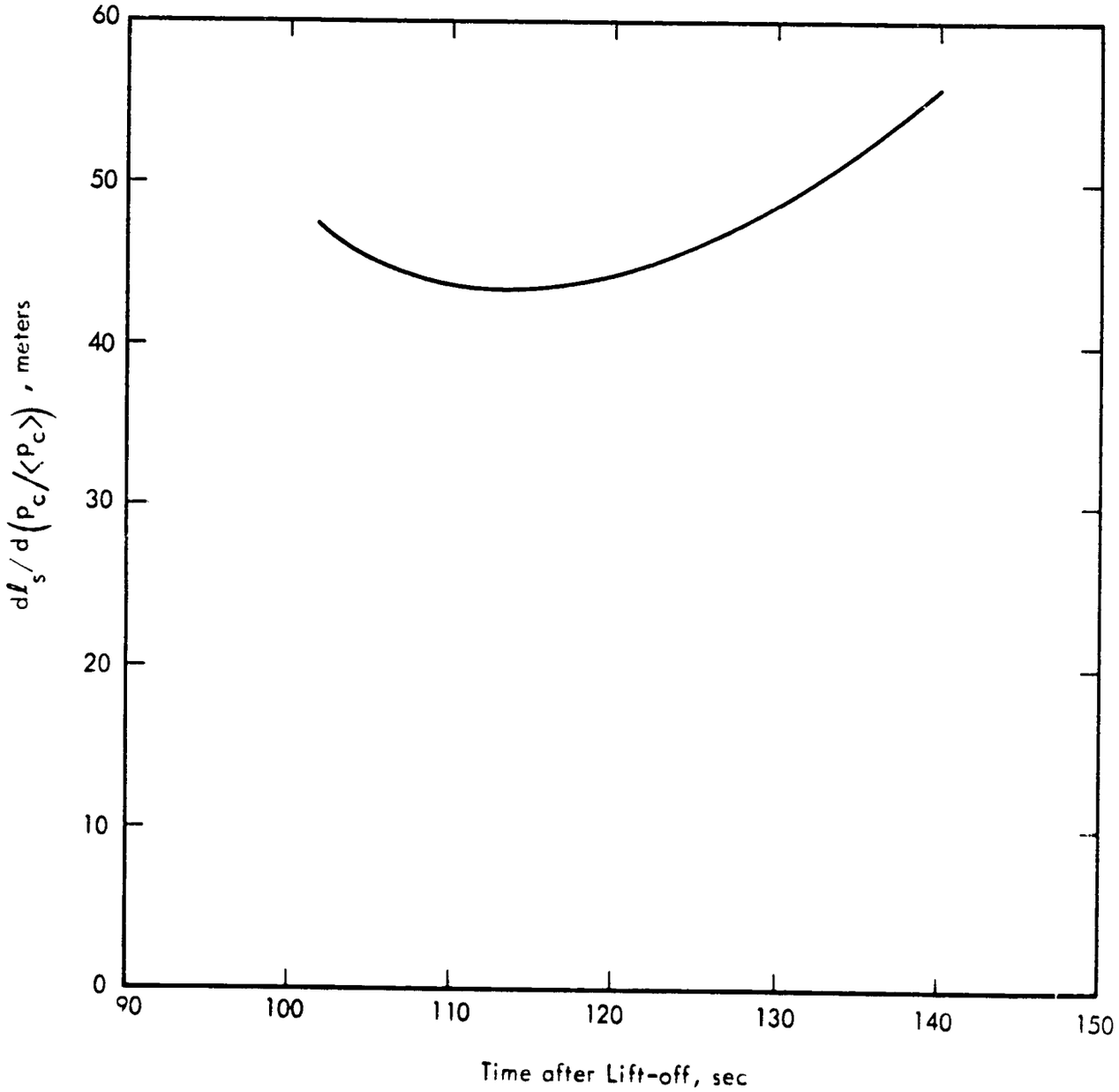

Figure 33. Change in Separation Length with Change in Engine Chamber Pressure for Shuttle SRB

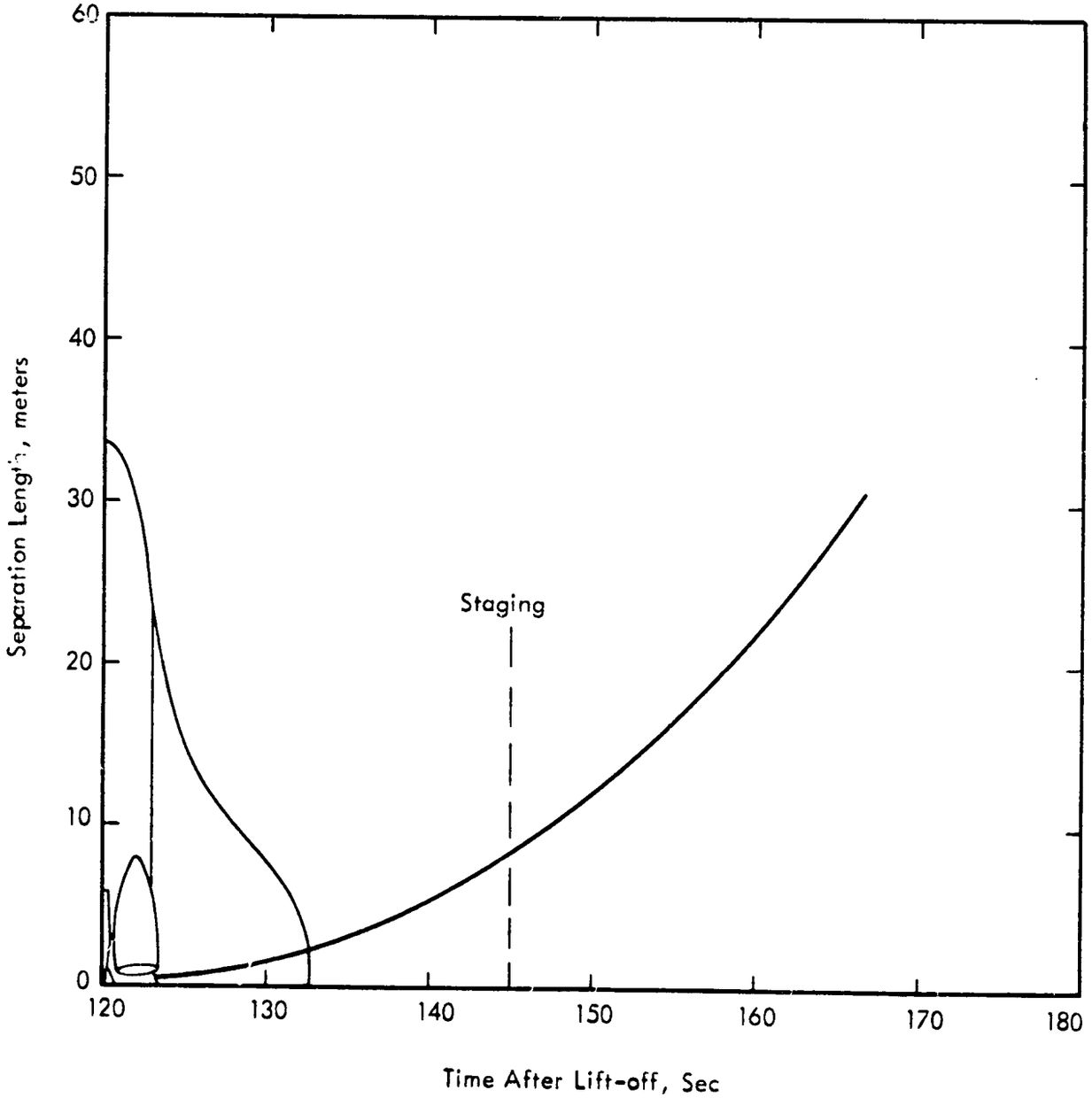

Figure 34. Prediction of Plume-Induced Separation Point on Shuttle Orbiter

APPENDIX A

DESCRIPTION OF COMPUTER PROGRAM 73/003P-1

WYLE LABORATORIES
COMPUTER PROGRAM DESCRIPTION

Program Number:	73/003P-1
Author:	K. J. Plotkin
Date:	February 1973
Source Language:	FORTRAN IV-H
Computer:	XDS Sigma V

1.0 PROGRAM TITLE

Plume Separation

2.0 PURPOSE

Given axisymmetric launch vehicle and trajectory parameters, the program computes properties relative to plume-induced separation. This includes separation length and plateau pressure, plus various properties of the plume and parameters describing the coupling to the unsteady pressure field.

3.0 METHOD

The analytic models incorporated in this program are described in detail in Wyle Laboratories Research Staff Report WR 73-3.

4.0 COMPUTER CONFIGURATION

The required hardware is: XDS Sigma V computer with 16 k core, card reader, and line printer.

5.0 PUNCHED CARD INPUT

Vehicle and trajectory parameters are input in metric units. Specific format for each card is as follows:

Card 1 — Descriptive title of vehicle. Up to 80 alphameric characters

Card 2 — Columns 1-10: Vehicle radius, meters
Columns 11-20: Total thrust, Newtons
Columns 21-30: Plume drag to thrust ratio
Columns 31-40: Exhaust gamma
Columns 41-50: Exhaust Mach number
Columns 51-60: Engine chamber pressure, N/m^2

Format for each item on this card is F10.0.

Card 3 — Descriptive title of trajectory. Up to 80 alphameric characters

Card 4 — N, the number of trajectory points to be read and computations performed for. Format I5.

Cards 5 through 4+N — Trajectory parameters

Columns 1-15: Time After Lift-Off, seconds
Columns 16-30: Altitude, kilometers
Columns 31-45: Flight Mach number
Columns 46-60: Free-stream dynamic pressure, N/m^2

Format for each item on these cards is E15.10.

6.0 OUTPUT

The first items output are a table of atmospheric properties and a table of separation conditions contained in the program. This is followed by output of the vehicle parameters contained in Card 2, prefaced by the title input in Card 1. The title input in Card 3 is then printed, followed by a listing of the trajectory parameters input. Five (5) tables of computed properties are then printed. Each of these tables consists of the time after lift-off, followed by various properties. The printout is sufficiently annotated so as to be self-explanatory; the column headings are FORTRAN representations of various expressions defined in WR 73-3. A sample output list is presented herein. Written below each column is the exact notation used in WR 73-3, or a definition for those items not specifically denoted in the report.

It should be noted that the program does not explicitly indicate whether or not the flow is separated. The output listing must be examined to determine this. The computed values represent separated flow when the plume angle is greater than the separation angle. In the sample output, flow is not separated at 84 seconds, but is at all other computation times.

ATMOSPHERE TABLE

ALTITUDE	PINF	RHOINF
0.	0.62000000E+05	0.12249994E+01
2000.	0.79501375E+05	0.10065994E+01
4000.	0.61660410E+05	0.81934994E+00
6000.	0.47218457E+05	0.66010997E+00
8000.	0.35651601E+05	0.52578997E+00
10000.	0.26499824E+05	0.41350996E+00
12000.	0.19399375E+05	0.31193995E+00
14000.	0.14170384E+05	0.22785997E+00
16000.	0.10352773E+05	0.16646999E+00
18000.	0.75652109E+04	0.12164998E+00
20000.	0.55293046E+04	0.88909983E-01
22000.	0.40474275E+04	0.64509987E-01
24000.	0.29717402E+04	0.46937998E-01
26000.	0.21883746E+04	0.34256998E-01
28000.	0.16161909E+04	0.25075998E-01
30000.	0.11970329E+04	0.18409997E-01
32000.	0.88906298E+03	0.11064998E-01
34000.	0.66341088E+03	0.98873992E-02
36000.	0.49852172E+03	0.72578974E-02
38000.	0.37713769E+03	0.53665973E-02
40000.	0.28714379E+03	0.39956979E-02
42000.	0.21996641E+03	0.29947999E-02
44000.	0.16949644E+03	0.22588998E-02
46000.	0.13134048E+03	0.17114098E-02
48000.	0.10229568E+03	0.13166999E-02
50000.	0.79779022E+02	0.10268997E-02
52000.	0.62228317E+02	0.80096977E-03
54000.	0.48491699E+02	0.63136988E-03
56000.	0.37657226E+02	0.49761985E-03
58000.	0.29137298E+02	0.39085978E-03
60000.	0.22466601E+02	0.30591990E-03

SEPARATION CONDITIONS - CONE

MACH NO	THETA SEP	P SEP	M SEP
1	0.26199996E+00	0.20000000E+01	0.10000000E+01
2	0.22699996E+00	0.20000000E+01	0.15299997E+01
3	0.19399994E+00	0.22119998E+01	0.24299993E+01
4	0.20899999E+00	0.28799991E+01	0.31199998E+01
5	0.22699999E+00	0.40000000E+01	0.36999998E+01
6	0.25299996E+00	0.57099990E+01	0.40000000E+01
7	0.27699998E+00	0.82969999E+01	0.43499994E+01
8	0.34999996E+00	0.11866999E+02	0.43499994E+01

SATURN V S-1

VEHICLE RADIUS =	5.03000	THRUST =	0.38000000E+08	D/T =	0.66400		
EXHAUST GAMMA =	1.23000	EXHAUST M =	3.70000	CHAMBER PRESSURE =	0.75000000E+07		

APOLLO NOMINAL TRAJECTORY

TIME	ALTITUDE	MACH NUMBER	DYNAMIC PRESSURE
84.	0.155999994E+02	0.209999943E+01	0.358840000E+05
96.	0.212999878E+02	0.275999928E+01	0.242770000E+05
10e.	0.2e0000000E+02	0.352999973E+01	0.142600000E+05
116.	0.330000000E+02	0.409999943E+01	0.926300000E+04
124.	0.365000000E+02	0.470999908E+01	0.573900000E+04
13e.	0.443999939E+02	0.537999916E+01	0.345000000E+04
14C.	0.508999939E+02	0.625000000E+01	0.207900000E+04
146.	0.561999969E+02	0.706999969E+01	0.135200000E+04

TIME	PLATEAU PRESSURE	SEPARATION ANGLE	PLUME ANGLE	PLUME RADIUS	SEPARATION LENGTH
84.	0.2246825768+05	0.2236999178+00	0.1514396678+00	0.4633998158+01	0.1894014368+01
96.	0.9667349228+04	0.2019179138+00	0.3004066568+00	0.5915404328+01	0.3942624338+00
108.	0.4147218848+04	0.2019452048+00	0.4416066628+00	0.7973199218+01	0.5388667038+01
116.	0.2322498788+04	0.2107999328+00	0.5281829838+00	0.1002663428+02	0.1062390718+02
124.	0.1363368148+04	0.2217799438+00	0.6088447578+00	0.1286967668+02	0.1747378548+02
132.	0.7526+11138+03	0.2364798458+00	0.6807737358+00	0.1671629338+02	0.2553066968+02
140.	0.4569309388+03	0.2594999078+00	0.7424497608+00	0.2166194158+02	0.3315829478+02
146.	0.3145710458+03	0.2539698798+00	0.7864379688+00	0.2695780948+02	0.3884481618+02

P_{sep} θ_{sep} θ_{pl} r_p ℓ_s

TIME	[illegible] RATIO	[illegible] LEVEL	[illegible]
8**	0.2[illegible]+01	0.1751[illegible]+03	0.3163[illegible]
9**	0.2161[illegible]+01	0.1488[illegible]+03	0.2183[illegible]
10**	0.2566[illegible]+01	0.1626[illegible]+03	0.1774[illegible]
11**	0.2991[illegible]+01	0.1577[illegible]+03	0.1469[illegible]
12**	0.3671[illegible]+01	0.1535[illegible]+03	0.1653[illegible]
13**	0.4649[illegible]+01	0.1494[illegible]+03	0.1712[illegible]
14**	0.6456[illegible]+01	0.1457[illegible]+03	0.1852[illegible]
14**	0.9546[illegible]+01	0.1427[illegible]+03	0.2054[illegible]

$\frac{P_{sep}}{P_\infty}$ $\quad 20 \log_{10} \frac{P_{sep}}{P_{ref}}$ $\quad \frac{P_{sep}}{q_\infty}$

$P_{ref} = 2 \times 10^{-5}$ N/m^2

TIME	D(THETA)/D(P/Q)	ROUT	D(LS/L)/D(THETA)	D(LSEP)/D(P/Q)
84.	0.3[illegible]E+00	-0.[illegible]E+00	0.[illegible]E+02	-0.11760E+02
96.	0.[illegible]E+00	0.23795[illegible]E+00	0.11[illegible]E+02	0.11[illegible]E+01
108.	0.[illegible]E+00	0.19[illegible]E+01	0.54[illegible]E+01	0.54[illegible]E+01
118.	0.[illegible]E+00	0.[illegible]E+01	0.[illegible]E+01	0.[illegible]E+01
124.	0.[illegible]E+00	0.[illegible]E+01	0.[illegible]E+01	0.10[illegible]E+02
134.	0.[illegible]E+00	0.[illegible]E+01	0.[illegible]E+01	0.12[illegible]E+02
144.	0.[illegible]E+00	0.[illegible]E+02	0.[illegible]E+01	0.14[illegible]E+02
146.	0.[illegible]E+00	0.[illegible]E+02	0.[illegible]E+01	0.[illegible]E+02

$$\frac{d\theta_{pl}}{d(p/q_\infty)} \qquad r_p \cos\left(\theta_{sep} + \theta_{reat}\right) - r_v \qquad \frac{1}{ROUT}\,\frac{d\,\ell_s}{d\,\theta_{pl}} \qquad \frac{d\,\ell_s}{d(p/q_\infty)}$$

TIME	D(TH1)/D(PC)	D(LSEP1)/D(PC)	D(LSEP1)/D(PC)
84.	0.1028[illegible]+01	-0.1932912[illegible]+01	-0.4385[illegible]+02
96.	0.9183865[illegible]+00	0.1475541115+01	0.6659911928+01
108.	0.8261394128+00	0.2422651[illegible]+01	0.1846046455+02
116.	0.7717[illegible]+00	0.2544243[illegible]+01	0.2366351325+02
124.	0.7229[illegible]+00	0.2538[illegible]+01	0.2914447025+02
136.	0.6797[illegible]+00	0.2402211195+01	0.3513444525+02
140.	0.6425[illegible]+00	0.2153229[illegible]+01	0.4073[illegible]
146.	0.6174[illegible]+00	0.1[illegible]+01	0.4524[illegible]

NSTOP

$$\frac{d\theta_{p1}}{d\left(P_c / \langle P_c \rangle\right)} \qquad \frac{\partial \ell_s}{\partial r_p} \qquad \frac{d\ell_s}{d\left(P_c / \langle P_c \rangle\right)}$$

WYLE WR 73-3

PREDICTION OF FLUCTUATING PRESSURE ENVIRONMENTS ASSOCIATED WITH PLUME-INDUCED SEPARATED FLOW FIELDS

Kenneth J. Plotkin, May 1973
Wyle Laboratories, Research Staff, Huntsville, Alabama

The separated flow environment induced by underexpanded rocket plumes during boost phase of rocket vehicles has been investigated. A simple semi-empirical model for predicting the extent of separation was developed. This model offers considerable computational economy as compared to other schemes reported in the literature, and has been shown to be in good agreement with limited flight data. The unsteady pressure field in plume-induced separated regions was investigated. It was found that fluctuations differed from those for a rigid flare only at low frequencies. The major difference between plume-induced separation and flare-induced separation was shown to be an increase in shock oscillation distance for the plume case. The prediction schemes were applied to PRR shuttle launch configuration. It was found that fluctuating pressures from plume-induced separation are not as severe as for other fluctuating environments at the critical flight condition of maximum dynamic pressure.

I. PLOTKIN, K.J.
II. WR 73-3
III. NAS8-26919

1. Rocket Exhaust Plumes
2. Separated Flow
3. Space Shuttle
4. Fluctuating Pressures
5. Prediction Methods

WYLE WR 73-3

PREDICTION OF FLUCTUATING PRESSURE ENVIRONMENTS ASSOCIATED WITH PLUME-INDUCED SEPARATED FLOW FIELDS

Kenneth J. Plotkin, May 1973
Wyle Laboratories, Research Staff, Huntsville, Alabama

The separated flow environment induced by underexpanded rocket plumes during boost phase of rocket vehicles has been investigated. A simple semi-empirical model for predicting the extent of separation was developed. This model offers considerable computational economy as compared to other schemes reported in the literature, and has been shown to be in good agreement with limited flight data. The unsteady pressure field in plume-induced separated regions was investigated. It was found that fluctuations differed from those for a rigid flare only at low frequencies. The major difference between plume-induced separation and flare-induced separation was shown to be an increase in shock oscillation distance for the plume case. The prediction schemes were applied to PRR shuttle launch configuration. It was found that fluctuating pressures from plume-induced separation are not as severe as for other fluctuating environments at the critical flight condition of maximum dynamic pressure.

I. PLOTKIN, K.J.
II. WR 73-3
III. NAS8-26919

1. Rocket Exhaust Plumes
2. Separated Flow
3. Space Shuttle
4. Fluctuating Pressures
5. Prediction Methods

WYLE WR 73-3

PREDICTION OF FLUCTUATING PRESSURE ENVIRONMENTS ASSOCIATED WITH PLUME-INDUCED SEPARATED FLOW FIELDS

Kenneth J. Plotkin, May 1973
Wyle Laboratories, Research Staff, Huntsville, Alabama

The separated flow environment induced by underexpanded rocket plumes during boost phase of rocket vehicles has been investigated. A simple semi-empirical model for predicting the extent of separation was developed. This model offers considerable computational economy as compared to other schemes reported in the literature, and has been shown to be in good agreement with limited flight data. The unsteady pressure field in plume-induced separated regions was investigated. It was found that fluctuations differed from those for a rigid flare only at low frequencies. The major difference between plume-induced separation and flare-induced separation was shown to be an increase in shock oscillation distance for the plume case. The prediction schemes were applied to PRR shuttle launch configuration. It was found that fluctuating pressures from plume-induced separation are not as severe as for other fluctuating environments at the critical flight condition of maximum dynamic pressure.

I. PLOTKIN, K.J.
II. WR 73-3
III. NAS8-26919

1. Rocket Exhaust Plumes
2. Separated Flow
3. Space Shuttle
4. Fluctuating Pressures
5. Prediction Methods

WYLE WR 73-3

PREDICTION OF FLUCTUATING PRESSURE ENVIRONMENTS ASSOCIATED WITH PLUME-INDUCED SEPARATED FLOW FIELDS

Kenneth J. Plotkin, May 1973
Wyle Laboratories, Research Staff, Huntsville, Alabama

The separated flow environment induced by underexpanded rocket plumes during boost phase of rocket vehicles has been investigated. A simple semi-empirical model for predicting the extent of separation was developed. This model offers considerable computational economy as compared to other schemes reported in the literature, and has been shown to be in good agreement with limited flight data. The unsteady pressure field in plume-induced separated regions was investigated. It was found that fluctuations differed from those for a rigid flare only at low frequencies. The major difference between plume-induced separation and flare-induced separation was shown to be an increase in shock oscillation distance for the plume case. The prediction schemes were applied to PRR shuttle launch configuration. It was found that fluctuating pressures from plume-induced separation are not as severe as for other fluctuating environments at the critical flight condition of maximum dynamic pressure.

I. PLOTKIN, K.J.
II. WR 73-3
III. NAS8-26919

1. Rocket Exhaust Plumes
2. Separated Flow
3. Space Shuttle
4. Fluctuating Pressures
5. Prediction Methods